Acta Pharmaceutica Sinica B 2021;11(5):1175−1199

Chinese Pharmaceutical Association
Institute of Materia Medica, Chinese Academy of Medical Sciences

Acta Pharmaceutica Sinica B

www.elsevier.com/locate/apsb
www.sciencedirect.com

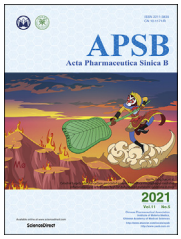

REVIEW

Synergistic integration of metal nanoclusters and biomolecules as hybrid systems for therapeutic applications

Peng Gao[a,b,*], Xin Chang[c], Dagan Zhang[a,b], Yafei Cai[d], Gen Chen[e], Hao Wang[f], Tianfu Wang[a,*]

[a]*Guangdong Key Laboratory of Biomedical Measurements and Ultrasound Imaging, Department of Biomedical Engineering, Shenzhen University, Shenzhen 518060, China*
[b]*State Key Laboratory of Bioelectronics, School of Biological Science and Medical Engineering, Southeast University, Nanjing 210096, China*
[c]*Key Laboratory of Biomedicine in Gene Diseases and Health of Anhui Higher Education Institutes, College of Life Sciences, Anhui Normal University, Wuhu 241000, China*
[d]*College of Animal Science and Technology, Nanjing Agricultural University, Nanjing 210095, China*
[e]*School of Materials Science and Engineering, Central South University, Changsha 410083, China*
[f]*College of Energy, Soochow Institute for Energy and Materials Innovations, and Key Laboratory of Advanced Carbon Materials and Wearable Energy Technologies of Jiangsu Province, Soochow University, Suzhou 215006, China*

Received 26 July 2020; received in revised form 2 October 2020; accepted 13 October 2020

KEY WORDS

Metal nanoclusters;
Biomolecule;
Nanoparticles;
Hybrid system;
Synergistic properties;
Fluorescence;
Bioprobe;
Therapy

Abstract Therapeutic nanoparticles are designed to enhance efficacy, real-time monitoring, targeting accuracy, biocompatibility, biodegradability, safety, and the synergy of diagnosis and treatment of diseases by leveraging the unique physicochemical and biological properties of well-developed bio-nanomaterials. Recently, bio-inspired metal nanoclusters (NCs) consisting of several to roughly dozens of atoms (<2 nm) have attracted increasing research interest, owing to their ultrafine size, tunable fluorescent capability, good biocompatibility, variable metallic composition, and extensive surface bio-functionalization. Hybrid core−shell nanostructures that effectively incorporate unique fluorescent inorganic moieties with various biomolecules, such as proteins (enzymes, antigens, and antibodies), DNA, and specific cells, create fluorescently visualized molecular nanoparticle. The resultant nanoparticles possess combinatorial properties and synergistic efficacy, such as simplicity, active bio-responsiveness, improved applicability,

*Corresponding authors.
E-mail addresses: pgao116@126.com (Peng Gao), tfwang@szu.edu.cn (Tianfu Wang).
Peer review under responsibility of Chinese Pharmaceutical Association and Institute of Materia Medica, Chinese Academy of Medical Sciences.

https://doi.org/10.1016/j.apsb.2020.12.004

and low cost, for combination therapy, such as accurate targeting, bioimaging, and enhanced therapeutic and biocatalytic effects. In contrast to larger nanoparticles, bio-inspired metal NCs allow rapid renal clearance and better pharmacokinetics in biological systems. Notably, advances in nanoscience, interfacial chemistry, and biotechnologies have further spurred researchers to explore bio-inspired metal NCs for therapeutic purposes. The current review presents a comprehensive and timely overview of various metal NCs for various therapeutic applications, with a special emphasis on the design rationale behind the use of biomolecules/cells as the main scaffolds. In the different hybrid platform, we summarize the current challenges and emerging perspectives, which are expected to offer in-depth insight into the rational design of bio-inspired metal NCs for personalized treatment and clinical translation.

1. Introduction

Abnormalities in biological systems, such as gene mutations, protein deficiency, pathogen infections (*e.g.*, Coronavirus disease 2019), immunity disorders, and tumoral metastasis have considerably threatened human health and economic development due to intrinsic complexity and variability[1]. Encouraged by the current technical advancements in bio-nanotechnology, bio-nanomaterials, as therapeutic agents, provide an enhanced therapeutic effect, accurate targeting, real-time monitoring, biosafety, prominent reproducibility, and clinical translatability[2,3]. Inspired by the biological systems, biomimetic strategies innovatively generate organic−inorganic hybrid composites with highly ordered hierarchical structures to address biomedical issues, which efficiently incorporate highly active biomolecules/cells with the unparalleled photonic, electronic, and catalytic features of metal components[4,5]. For personalized medicine, the size, composition, and physicochemical properties of nanomaterials can be manipulated, or their surface can be functionalized by biomolecules or specific cells with stealth and targeting therapeutic effect[6,7]. For example, Conde's group[8] reported that gold nanoparticles with the combination properties of gene, drug and phototherapy were readily delivered through a prophylactic hydrogel patch and led to tumor remission in a colon cancer mouse model. In addition, the physicochemical and physiological properties of sub-micrometer-sized materials (1−1000 nm) can further be programmed by tuning parameters, such as size, charge, shape, structure, and surface properties, thus supporting diverse therapeutic applications in living organisms[5,6,9]. Nevertheless, the biocompatibility of these bio-nanomaterials is a demanding challenge during treatment. Rapidly developed nanostructured materials, especially larger metal nanoparticles (NPs) with generally higher stability, non-biodegradability, and unpredictable release, have been severely hampered by the toxicity induced by their nonspecific accumulation in the reticuloendothelial system (RES), immune clearance, and the lack of spatial and temporal control over their biological activities[10−12]. Therefore, developing bio-inspired NPs with ultrafine size, excellent biocompatibility, and multifunctionality by converging nanoscience, interfacial chemistry, and biotechnology is highly promising for therapeutic purposes.

Ultrasmall bio-inspired metal nanoclusters (NCs) offer an elegant solution due to typical biomolecule shell−metal core structures and molecule-like properties, indicating great potentials for therapeutic applications[13−15]. In such a hybrid system, metal NCs composing of several dozens of atoms (< 2 nm) exhibit strong quantum confinement effect and discrete electronic state, which is capable of generating size-dependent fluorescence and physicochemical properties regulated by the sub-nanometer sizes and structures of different metal cores. Considerable progress has been made in the controllable synthesis of atomically precise metal NCs, including Au, Ag, Cu, Pt, Pd, Cd, Bi, and Mo, as well as alloy NCs comprising two or more species of metal atoms[13,16−20]. Meanwhile, a variety of biomolecules (*e.g.*, DNA, peptides, and proteins) and specific cells have been successfully exploited as ligands for the synthesis of various metal NCs because of their tunable biomolecular sequence and 3D structures, excellent biocompatibility, and variable bioactivities. Bioimaging to obtain information on precise pathological changes requires the use of more dynamic molecular imaging probes capable of identifying significant features of diseases. Compared with semiconductor quantum dots (QDs)[21,22], organic fluorophores[23], and fluorescent proteins[24], biomolecule-mediated metal NCs exhibit an array of advantages, which include ultrafine size, ease of fabrication, improved photophysical properties, low toxicity, extensive functionality, and facile tailorability, which make them powerful alternatives to optically guided therapeutic NPs[25−27]. In contrast to larger metal NPs, bio-inspired metal NCs with ultrafine size, structure, and surface functionality facilitate *in vivo* real-time monitoring, bio-responsiveness, controlled dose, and renal clearance without severe side effects which prevents their huge accumulation in the liver and spleen[28−30]. Moreover, metal-based drugs have been explored for their therapeutic performance, such as US Food and Drug Administration (FDA)-approved metallic drugs auranofin, a gold (I) compound used for the treatment of rheumatoid arthritis and cisplatin or *cis*-diamminedichloroplatinum (II) is used as a metal-based anticancer drug, have been explored for their therapeutic performance. To globalize precision medicine, bio-inspired metal NCs could be exploited as a universally therapeutic system to effectively integrate customizable biological effects (specificity, intrinsic bioactivity, and

biodegradability) and tunable physicochemical properties (size, structure, and composition)[31−33].

In the current review, we present a comprehensive discussion on bio-inspired metal NCs intended for various therapeutic applications, with an emphasis on the concept of utilizing biomolecules and cells as scaffolds. Considering the increasing importance of biomolecules and cells in the biopharmaceutical industry[34,35], bio-inspired metal NCs have motivated the production of multifunctional NPs with therapeutic, delivery, and dynamic tracking capabilities at the disease site by leveraging on their assembly capability and biological effects. From a material perspective, the purpose of this review is to deliver an in-depth understanding of the engineering of fluorescent bio-inspired metal NCs, such as bioprobes, radiosensitizers, photosensitizers, drug conjugates, nanovaccines, nanocarriers, antibacterial agents, and nanoenzymes for therapeutic applications (Fig. 1). Instead of providing a general historical survey of various metal NCs, the design rationale and therapeutic performance of previously reported therapeutic NCs are highlighted. Furthermore, we summarize the challenges associated with the therapeutic applications of bio-inspired metal NCs. Finally, we close with our perspective on the development of innovative bio-inspired metal NCs with reliable structure-related properties and combinatorial strategies and suggest new ideas for innovative design of visualized hybrid systems intended for clinical translation.

2. Characteristic biomolecules to control the synthesis of metal NCs and their functionalities

Biomolecules are effective in bringing desired properties of metal clusters due to characteristic sequences, tunable 3D structures, and extensive biofunction. Inspired by the biomolecular folding for the formation of biological function and micro/nano structure, numerous biomolecules (amino acids, peptides, proteins, and DNA) and their derivatives have been explored for the preparation of various metal NCs with three-dimensional hierarchical structures and extensive bio-functionalization. Generally, the assembly of bio-inspired metal NC is usually driven by various driving forces at nano-bio interactions, such as coordination chemistry, electrostatic interaction, van der Waals forces, hydrophobic interaction, hydrogen bonding, covalent bonding, host-guest interaction, and bio-specific interaction. On the one hand, atomically precise metal NCs can be creatively prepared by adjusting the type of biomolecule, the ligand-to-metal ratio, the strength of the reducing agent, and other experimental conditions, such as reaction temperature, solvent condition, and reaction time. On the other hand, the tunability and modulation of biomolecules facilitate the delicate combination of different domains, thus allowing the fabrication of metal NCs with diverse sizes, compositions, morphologies, geometry, hierarchical structures, and surface functionalities. Owing to their programmable, periodic, and biodegradable nature, the utilization, and customization of biomolecules is an attractive strategy for the construction of an array of metal NCs. This principle implies sufficient molecular control of the structure and properties of the NCs under physiological and pathological milieu, which is not obtainable with larger metal NPs. Based on biochemical driving forces, various synthesis strategies for the assembly of bio-inspired metal NCs have been summarized in the following section.

2.1. *Coordination chemistry*

The interfacial chemistry has developed advantageous structure−property−performance relations that are crucial for their biomedical applications due to the atomic level management of the size, structure, composition, and surface of metal NCs. Recent research has primarily focused on the synthesis of various metal NCs by using coordination chemistry as the main strategy[33,36−38].

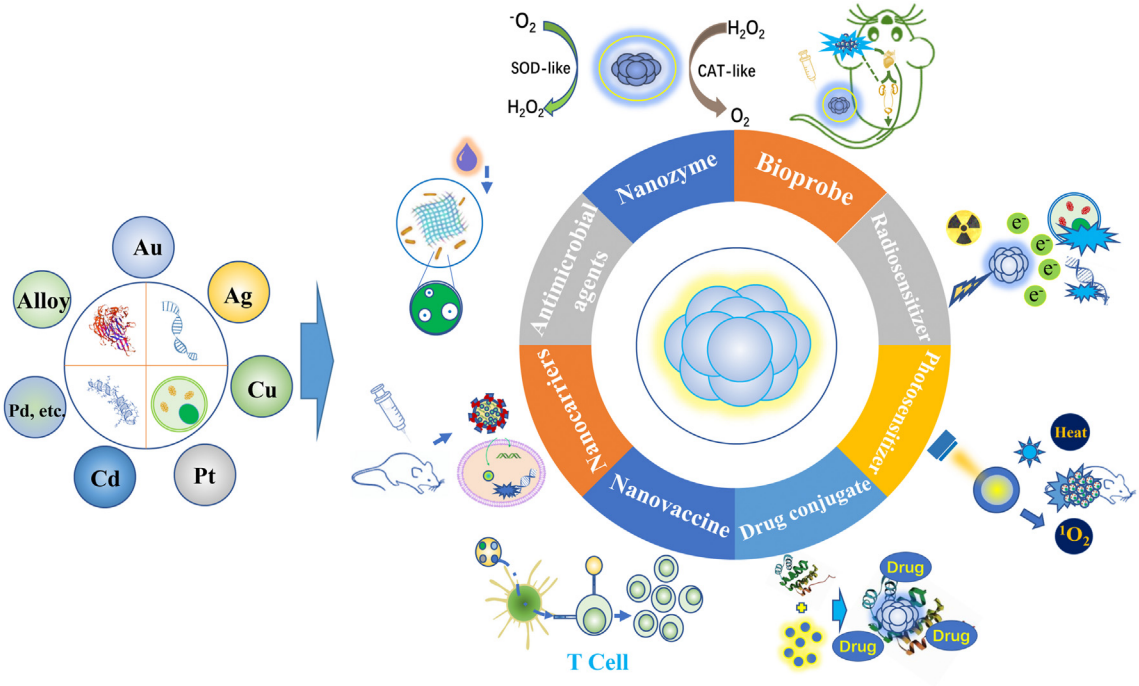

Figure 1 Schematic representation of bio-inspired metal nanoclusters and their therapeutic capability.

To a large extent, various biomolecules as stabilizing ligands to coordinate metal NCs have been extensively explored, such as proteins, peptides, DNA, and specific cells. Biomolecules facilitate for the controllable synthesis of metal NCs by their high metal-binding affinity, large steric hindrance, and matchable reducing effect. Generally, strong stabilizing agents and weak reducing agents collectively result in smaller-sized metal NCs at the molecular level, whereas excessive reduction leads to the formation of metal NPs without any fluorescence. Recent success in interfacial chemistry has yielded a great deal of metal NCs, including Au, Ag, Cu, and Pt NCs, as well as precisely doped NCs. As highlighted in a previous sensing review by our group, templates, and etching routes are mainly determined by the metal-ligand interaction of metal atoms and biomolecules in the synthesis of atomically precise metal clusters.

Similar to the biomineralization process, template routes mostly rely on functional biomolecules where they provide scaffolds for minerals followed by sequestering and immobilization of inorganic ions in closed spaces. Typically, Xie et al.[7] firstly employed bovine serum albumin (BSA) as a classic template to synthesize red-emitting BSA-Au_{25} NCs with a quantum yield of approximately 6%[7]. By using BSA as a reducing and stabilizing agent, Au NCs were facilely prepared *via* one-pot "green" synthesis method at reaction conditions of pH 12 and 37 °C. In light of this, this synthesis strategy for the fabrication of an array of metal NCs was widely adopted by using various proteins, enzymes, peptides, and DNA, such as lysozyme[39–42], apoferritin[43], pepsin[44], ribonuclease A[45], short peptides[46,47], and customized DNA[48]. Notably, lysozyme can be used to synthesize an array of different metal NCs with corresponding optical properties. Furthermore, using biomolecules as stabilizing ligands, variable metal NCs and alloy metal NCs can also be produced, indicating the possibility of modulating characteristic biomolecules to produce various metal NCs. For instance, Richards et al.[19] proposed a DNA microarray technology to obtain unique DNA sequence templates, and employed them to synthesize five kinds of fluorescent Ag NCs with blue, green, yellow, red, and near-infrared emissions. In contrast, various proteins/peptides collectively perform as both mild reducing agents and stabilized agents due to various reducing and stabilized groups, allowing the steric protection to form various stable metal NCs under appropriate conditions. Considering the impact of reduction force, mild reducing agents are universally adopted to improve the nucleation of metal atoms and the controllable synthesis of atomically precise metal NCs. In a typical case, by utilizing gaseous carbon monoxide (CO) as a mild reducing agent, Yu and co-workers[49] developed a simple one-pot method for the synthesis of thiolated $Au_{25}(Cys)_{18}$ NCs with high purity, large-scale production, and ~95% product yield. Some studies have also revealed the implication of the sequence-based and conformational variation of biomolecular templates in the synthesis and stabilization of metal NCs. In another case, Yu et al.[17] modulated BSA conformation to produce the isomeric forms of BSA, which were employed as templates to fabricate five-dimensionally discontinuous Au NCs (Au_4, Au_8, Au_{10}, Au_{13}, and Au_{25}) through CO mediated reduction. Furthermore, through a customized strategy, the rational design of biomolecular templates was proposed to prepare various metal NCs. For example, Wang's group[46] employed a bifunctional peptide containing a domain that targets cell nuclei and a domain with the ability to biomineralize and capture Au clusters. The as-prepared peptide-Au NCs exhibited red emission (λ_{em} = 677 nm) and specifically stain the nuclei of three cell lines. Aires et al.[50] proposed a simple and versatile approach to design histidine coordination sites into a protein structure for the sustainable synthesis of metal NCs, which is translatable to other proteins to obtain protein-encapsulated metal NCs for various biomedical applications. Specifically, the consensus tetratricopeptide repeat module, a 34 amino acid helix-turn-helix motif, was used as a study model for the synthesis of Au, Ag, or Cu NCs. Notably, this method could cause a destructive effect on conformation-related functions and bioactivities because the template route usually requires the unfolding of biomolecular conformation. In addition, specific cells can be selected to synthesize metal NCs. Chen et al.[51] proposed that biocompatible Pt NCs could be spontaneously biosynthesized by cancerous cells (HepG2 (human hepatocarcinoma), A549 (lung cancer), and others) rather than noncancerous cells (human embryo liver L02 cells). The method has been shown effective for inert structural proteins or short peptides that do not require complex structure and conformation-sustained bioactivities for therapeutic applications.

Ligand etching is an effective route to produce stable metal NCs in a controlled manner. The etching of metal NCs or NPs could be established for the formation of smaller metal NCs by manipulating a variety of biomolecules, such as amino acids, peptides, proteins, and DNA as etching ligands. For example, BSA was utilized to etch MSA-protected Au NPs, resulting in the formation of fluorescent Au_{38} NCs with a quantum yield of 4.0%[52]. Furthermore, Zhou et al.[53] fabricated a monodisperse atomic-levelprecise Au_8 NCs by etching Au nanocrystals (particles and rods) with BSA under ultrasonic aqueous conditions. In a similar study, luminescent Pt NCs was produced using GSH as the etchant. The Pt NCs exhibited an intense fluorescence signal (quantum yields = ~17%) in the yellow region, which can lead to the formation of blue-emitting species after a prolonged etching processing[54]. Despite the relatively few studies on the etching route, most studies have demonstrated that different biomolecules affects the etching process of metal NCs. For instance, through the phase transfer cycle (aqueous−organic−aqueous) of electrostatic interactions, Yuan et al.[20] employed a simple and scalable synthetic peptide to synthesize various metal (Ag, Au, Pt, and Cu) NCs with high fluorescence emission under moderate etching conditions. Among the NCs, Ag NCs protected by Asp-Cys-Asp, Glu-Cys-Glu, and Ser-Cys-Ser peptides exhibited strong red emissions, whereas synthetic Lys-Cys-Lys Ag NCs emitted intense blue color fluorescence under UV light. Afterwards, controllable size-focusing strategies have been adopted to achieve atomically precise metal NCs with great productivity. By using NaOH-mediated and NaBH4 reduction conditions, Yuan et al.[55] developed a controlled strategy to synthesize thiolated Au_{25} NCs using Cys, homocysteine (HCys), and GSH as the ligands. NaOH could effectively balance the growth and etching rate of metal NCs to complete fast size-focusing and good control of the generation process. However, non-physiological reaction conditions, such as organic solutions, sharp alkalinity, and high temperature could be detrimental to the pristine structure and function of biomolecules. Therefore, the mild aqueous assembly conditions with soft reducing agents make it possible to incorporate

biological molecules while avoiding solvents as well as temperature, pH values, and ionic strength that can destabilize the compounds.

2.2. *Chemical post-modification*

One attractive advantage of biomolecular ligands is the abundance of functional groups for the post-modification of metal NCs through carboxylic acids and amines. With glutaraldehyde or EDC/NHS (*N*-ethyl-*N*′-(3-(dimethylamino)propyl)carbodiimide/*N*-hydroxysuccinimide), functional biomolecules can readily functionalize metal NCs with desirable properties without compromising the bioactivities. In a typical case, Wang et al.[56] treated BSA-Au NCs with glutaraldehyde and subsequently conjugated it with trastuzumab (Herceptin). Herceptin-modified BSA-Au NCs successfully achieved nuclei targeting and enhanced therapeutic efficacy against cancer cells. A similar strategy to multiple-step post modification may also be used to prepare multifunctional metal NCs. Furthermore, multiple-step post modification may also be a useful attempt for the construction of multifunctional metal NCs. In light of this, Khlebtsov et al.[57] proposed an Au NC-based complex with various properties, including imaging, targeting, and photodynamic therapy (PDT) against *Staphylococcus aureus*. To achieve this, highly fluorescent BSA-Au NCs were conjugated with immunoglobulin G (IgG) through EDC chemistry, and the surface was further modified with a commercial photosensitizer. In another study, live NIH 3T3 cells were stained with avidin-C_{24}-Ag NCs or anti-heparin sulfate-C_{24}-Ag NCs, revealing the effective internalization based on avidin-biotin or antibody-antigen interaction[58]. Current review shows that newly developed functional nanomaterials could be readily used to modify bio-inspired metal NCs for improved efficacy without compromising their biological activities and fluorescent properties, thus achieving multifunctionality for wide therapeutic purposes.

2.3. *Molecular assembly*

Inspired by a wide variety of cellular nanostructures (*e.g.*, actin filaments, microtubules, vesicles, and micelles), molecular assembly is a promising strategy to manipulate the spatial arrangement of nanosized building blocks to form specific structures and morphology, from the nanoscale to the macroscale[37,59,60]. In addition to coordination chemistry, non-covalent binding, including hydrogen bonding, electrostatic interaction, hydrophobicity, and $\pi-\pi$ stacking, is mediated primarily by the molecular assembly to achieve diverse morphology and functionality. The few attempts to carry out ordered assembly of metal NCs over large areas have been successful. For instance, an abundant, low-cost, and sustainable plant protein, the pea protein isolate (PPI), was selected as both a reducing and stabilizing agent to facilely produce Au NCs exhibiting a strong red fluorescence and outstanding stability. The formed Au NCs/PPI mixture was able to self-assemble into Au NCs/PPI NPs with a size of ~100 nm because of the change in the surface charging of the PPI during the dialysis process[61]. Characteristic biomolecules may assist the formation of nanoarchitecture by supplying additional hydrophobic attraction. In light of this, Zhang et al.[62] designed self-assembling peptides as a novel bio-inspired scaffold to produce gold NCs. The resulting Au NCs capped with motif-designed peptides undergo controlled supramolecular self-assembly to form nanofiber structures, in which the luminescence of Au NCs is significantly enhanced by nearly 70-fold, with 21.3% quantum yield. For biosensing applications, Nair and coworkers[63] designed a fluorescent probe by mixing new near-infrared (NIR)-emitting GSH-Au NCs with urease to specifically target urea. The successful physical entrapment of Au NCs within urease was determined by observing the fluorescence spectral data, which exhibited an accurate measurement of the blood urea level in whole blood and blood serum. Besides, a cationic polyelectrolyte, poly(diallyldimethylammonium chloride), was used to modify fluorescent DNA-Ag NCs, resulting in 3-fold fluorescence emission enhancement *via* electrostatic interaction between the positive polymer backbones and the negatively charged phosphate groups of DNA strands[64]. In addition to the effect of stabilizing for metal NCs, characteristic biomolecules to could be designed to facilitate the subsequent self-assembly of metal NCs into superstructures with diverse morphologies and symmetries, thus allowing a reversible response to external stimuli (pH, temperature, and solvent).

3. Combinatorial properties of bio-inspired metal NCs for therapeutic applications

Characteristic biomolecules are used to mediate the synthesis, assembly, and bio-functionalization of metal NCs with integrated structures and molecule-like behavior. The integration of metal NCs with biomolecules could effectively integrate unique optical, electronic, and catalytic properties with biological features, unprecedentedly creating synergistic or even unexpected effects for therapeutic applications. The combinatorial properties of bio-inspired metal NCs provide functional NPs with enhanced therapeutic efficiency and consistent spatiotemporal delivery. On the one hand, instead of exhibiting continuous energy level and behaving as conductors, few-atom metal NCs exhibit discrete energy level, and their optical properties are determined by their size, chemical state, composition, structures with tunable fluorescence, intensity, quantum yield, high photothermal conversion efficacy, and other therapeutic performance. The inorganic module harbors multiple interesting properties that can be applied for the treatment of various diseases. On the other hand, biomolecules that can be combined with various functional groups can confer specific functionalities on the surface of metal NCs, such as targeting and therapeutic properties. In this regard, bio-inspired metal NCs have a structure−property relationship, which makes them an invaluable tool to facilitate combinatorial physicochemical and biological properties for catalytic, medical, and environmental applications. Looking at the current progress, we systemically discuss various factors that influence the physicochemical properties of bio-inspired metal NCs and their functional behavior in the following section.

3.1. *Size and structural effects*

Metal NCs are typically composed of dozens of atoms, between a single atom and metal NPs, which are characterized by strong quantum confinement effect and discrete energy levels. When interacting with light, metal NCs allow energy electron transitions and produce fluorescent emission from the visible to the near-infrared region[65]. The atomic structure of metal NCs and their electronic behavior drastically change when the size of NPs is reduced to the sub-2 nm regime. Notably, recent studies have indicated that metal species, size, structure, oxidation state, and

coating ligands collectively contribute to their physicochemical properties. According to previous study, water-soluble atomic precise gold NCs with various compositions were successfully synthesized, including $Au_{15}(SG)_{13}$, $Au_{18}(SG)_{14}$, $Au_{22}(SG)_{16}$, $Au_{22}(SG)_{17}$, $Au_{25}(SG)_{18}$, $Au_{29}(SG)_{20}$, $Au_{33}(SG)_{22}$, and $Au_{39}(SG)_{24}$[66,67]. Among the NCs, $Au_{25}(SR)_{18}$ has received the most extensive attention from material scientists. Yu et al.[68] successfully synthesized atomically accurate thiolated gold NCs $Au_{22}(SG)_{18}$ using carbon monoxide reduction, which has a strong fluorescence emission at 665 nm (λ_{ex} = 520 nm) with a quantum yield of approximately 8%. Compared with $Au_{25}(SG)_{18}$, which differs only by 3 Au atoms, $Au_{22}(SG)_{18}$ showed significantly different fluorescence properties. Although it exhibited a similar fluorescence emission wavelength, the fluorescence was weaker and the quantum yield was only approximately 0.2%. The geometric configuration of the metal NCs also affected its optical properties. Typically, both $Au_{25}(SC_2H_4Ph)_{18}$ and $[Au_{25}(PPh_3)_{10}(SC_2H_5)_5Cl_2](SbF_6)_2$, which both contain 25 gold atoms, displayed significantly different optical properties. By comparison, the former has a double icosahedral structure, while the latter has a core−shell structure-nuclear icosahedral Au_{13} core and six S-Au-S-Au-S "staple"-like shell structures. Based on density functional theory, the fluorescence of $[Au_{25}(PPh_3)_{10}(SC_2H_5)_5Cl_2](SbF_6)_2$ was derived from the inter-band transition of two icosahedrons sharing the apex, whereas the fluorescence of $Au_{25}(SC_2H_4Ph)_1$ was from the band (*sp-sp*) transition, and its lowest possession electron energy level was 1.8 eV. Furthermore, the well-defined sizes and structures of $Ag_{16}(SG)_9$ and $Ag_9(SG)_6$ exhibit excellent stability and different fluorescence emission in the aqueous phase[69]. Mono-doped NCs were also analyzed because their optical behaviors displayed significant differences from those of the undoped NCs. To explain this, Bootharaju et al.[70] conducted a comparative study on the fluorescence of Ag_{25}, Pd_1Ag_{24}, and Au_1Ag_{24}, and found that the fluorescence emission intensity of Au_1Ag_{24} was ~25 times higher than that of Ag_{25}. Furthermore, the oxidation state of the metal NCs and the alloy composition affected their optical properties. For example, the bimetallic Au-Ag NCs exhibited significant red fluorescence enhancement with 6.5- and 4.7-fold higher fluorescence intensity than the conventional Au NCs and core−shell Au@Ag NCs, respectively. Although the same doses of Au and Ag precursors were used, the fluorescence intensity of the alloyed Au−Ag NCs was much higher than that of the core−shell Au@Ag NCs. The compositional test indicated that the alloyed Au−Ag NCs consisted of Au(0) and Ag(I)/Ag(0), while the core−shell Au@Ag NCs consisted of Au(I) and Ag(0)[71]. The metallic cores in a reduced state could enhance the efficiency of charge transfer and result in stronger fluorescence intensity. In addition, it has also been shown that the protecting ligand influences the fluorescence of NCs based on the electronic interactions and the electron-donating ability of the ligand[72]. In view of this, fluorescent emission intensity could be effectively enhanced by adopting ligands with electron-rich groups or increasing the ligand-metal ratio[73]. All the aforementioned factors collectively determine the physicochemical properties of bio-inspired metal NCs and favor the future design for therapeutics.

3.2. *Optical absorption*

Metal NCs produce electronic transitions between energy levels by interacting with light, resulting in the sharp absorption of ultraviolet−visible (UV−Vis) light. Well-defined metal NCs are considered to possess characteristic absorption features that can be distinguished from each other. For example, Zhu et al.[74] found that glutathione (GSH)-stabilized Au_{25} exhibited specific absorption peak characteristics in the 400−1000 nm range, which were considered as in-band (sp←sp) or inter-band (sp←d) transition. The absorption spectrum of $Au_{15}(SG)_{13}$ is approximately 370 nm and the band gap is approximately 2.5 eV. The UV−Vis spectra of $Au_{18}(SG)_{14}$ showed different bands of absorption peaks at 390 and 562 nm, a wide shoulder band at 620 nm, and a band gap of approximately 1.8 eV. The $Au_{38}(SC_2H_4Ph)_{24}$ is highly spectrally structured with multiple bands at 1050, 745, 620, 560, 520, and 490 nm, and the band gap is approximately 0.9 eV[75]. Notably, Negishi et al.[76] have demonstrated that as the particle size decreases, the interval between the discrete states of each band increases, thus resulting in a blue shift of the absorption peak. In addition to Au NCs, Petty et al.[77] reported that gamma-fluorescent Ag NCs have significant UV−Vis absorption at 357 and 440 nm. Meanwhile, DHLA-protected Ag_4 and Ag_5 exhibited significant absorption peaks at 335 and 435 nm, and the other shoulder peak at 500 nm[78]. In another study, Baksi et al.[79] showed that $Ag_{11}(SG)_7$ has an absorption peak 19 at 485 and 625 nm. Apart from Au NCs and Ag NCs, Cu NCs with absorption peak in the UV region (307 nm) were reported[80]. In addition, using UV−Vis absorption spectroscopy, characteristic absorption of PEI-encapsulated Pt NCs were observed at 350 nm[81].

3.3. *Fluorescence emission*

Photoluminescence is one of the most attractive properties of metal NCs in therapeutic applications. Because of the discrete energy levels rather than the continuous energy state of metal NPs, metal NCs exhibit molecular-like transitions (HOMO−LUMO transition) by interacting with light, resulting in sharp fluorescent emission from the visible to the near-infrared region. Generally, fluorescence properties include emission, excitation, Stokes shift, luminescence lifetime, and photostability. It should be noted that the luminescence lifetime of metal NCs is much longer than that of organic dyes, up to 100 ns or even longer. To our knowledge, major factors, including the core size, protecting ligand, valence electron count, the oxidation state of the metal, crystal structure, and the synthetic condition are closely associated with the regulation of the PL behavior[14]. As such, good photostability, strong luminescence with microsecond luminescence lifetime, large Stokes shift (>200 nm), and NIR emission, are beneficial for bioimaging. Currently, a variety of fluorescent mechanisms for metal NCs have been proposed. Huang et al.[82] believed that the luminescence of monolayer-protected gold NCs is closely associated with the inter-orbital transition between the *d* orbital and the *sp* orbital. Furthermore, Link et al.[83] ascribed red fluorescence emission of GSH-stabilized Au_{25} NCs to the energy transfer between HOMO−LUMO, which originated from the transition within sp orbital. Moreover, Huang et al.[84], showed that Au NCs exhibited large Stokes shift and long fluorescence lifetime (>100 ns), which was attributed to the charge transfer between the ligand and metal in thiol−gold (I) complex. $Au_{28}(GS)_{16}$ NCs proposed by Huang and Murray[85] showed singlet fluorescence and triplet phosphorescence. Therefore, it is believed that the luminescence of monolayer-protected Au NCs is closely related to the orbital transition between the *d* orbital and the *sp* orbital. The observed long-wave fluorescence might be ascribed to the charge transfer process of the organic ligand shell. Wu et al.[72] demonstrated that the sulfhydryl-protected ligands have an important role in the

fluorescence emission of gold NCs. They confirmed that the luminescence mechanism was affected by factors such as the size and composition of the gold NCs, the ligands on the surface, and the synthetic route; however, there is no definite evidence to confirm the mechanism of fluorescence generation by Au NCs. In addition, it was hypothesized that the surface ligands influenced PL intensity in two ways: (i) charge transfer from the ligands to the metal NCs kernel through metal−S interactions; and (ii) direct donation of delocalized electrons from electron-rich atoms (or groups) on the ligands to the metallic kernel. Therefore, the unique structure and tunable fluorescence properties of metal NCs make them highly sensitive and selective to the surrounding biological cues.

3.4. *Two-photon excited fluorescence*

Two-photon absorption (TPA) refers to the simultaneous absorption of two photons with the same or different frequencies to excite a molecule from a state (usually the ground state) to a higher-energy electronic state. A wide spectrum of metal NCs shows the capability of TPA, which is especially suitable for *in vivo* imaging and PDT[86]. Compared to single-photon excitation, two-photon excitation in two near-infrared regions increased penetration depth and spatial resolution due to lower scattering and sample auto-fluorescence advantages. To understand the inherent relationship between metal cluster size and nonlinear optical properties, Ramakrishna et al.[87] used *n*-hexane thiol as a passivator to synthesize a series of Au NCs containing 25, 140, 309, 976, and 2406 atoms. Their comparative experiments confirmed that Au_{25} NCs were very good TPA materials and the TPA cross-sectional area was 2700 GM (opert-Mayer unit, 10^{-50} $cm^4 \cdot s$) at 1290 nm. Regarding multi-photon imaging, Polavarapu et al.[88] reported that GSH-stabilized Au NCs have strong single-photon and two-photon emission characteristics with excellent optical stability. Their TPA cross-section is 189,740 GM, which shows a much larger cross-section than organic fluorescent dyes and QDs. In addition, Patel et al.[89] demonstrated that the water-soluble ssDNA-Ag NCs achieved a two-photon cross-section of 50,000 GM with high quantum yields in both the red and near-infrared regions. In this process, Ag NCs emitting at 660, 680, or 710 nm exhibited a larger two-photon cross-section than water-soluble semiconductor QDs. Isabelle et al.[90] reported that $Ag_{29}(DHLA)_{12}$ exhibited a TPA cross-section above 104 GM at approximately 800 nm. Compared with the single-photon excitation spectrum, their two-photon excitation fluorescence spectrum showed a strong blue shift at a bandwidth between 400 and 700 nm. In addition, Wang et al.[91] designed bifunctional peptide-stabilized Cu NCs as probes for nuclear labeling. The Cu NCs mainly consisted of Cu_{14} and emitted blue two-photon fluorescence emission under a femtosecond laser excitation. Such properties greatly facilitate the controllability of metal NCs, which is crucial for perceiving the precise structure and crystallization of metal NCs at the atomic level.

3.5. *Aggregation-induced luminescence (AIE)*

Luminescent materials with AIE properties have attracted much interest through the principle of restriction of intramolecular rotations since the debut of the AIE concept in 2001. The development of AIE-based metal NCs with tunable emission and enhanced intensity is necessary in both fundamental and applied research[92,93]. Regarding the luminescence fundamentals of metal NCs, a recent study showed that the emission wavelength of Au NCs is adjustable from the visible region to the NIR-II region by controlling the length of the AuI-SR motifs on the NC surface. In view of this, decreasing the length of AuI-SR motifs also changes the origin of cluster luminescence from AIE-based phosphorescence to Au^0-core-dictated fluorescence[94]. In another case, the self-assembly of NCs was initiated by surface-motif reconstruction of $[Au_{25}(SR)_{18}]$ from short SR-$[AuI\text{-}SR]_2$ units to long SR-$[AuI\text{-}SR]_x$ ($x > 2$) staples accompanied by structural modification of the intrinsic Au_{13} kernel, which facilitated the self-assembly of Au NCs into well-defined nanoribbons in solution. Notably, the compact structure and effective aurophilic interactions within the nanoribbons significantly enhanced the luminescence intensity of Au NCs, with an increased quantum yield of 6.2% at room temperature[95]. AIE properties are also applicable to various M(I)-thiolate complexes (M = Au, Ag, Cu, etc.) and the spectral features of the aggregated M(I)-thiolate complex closely resemble that of highly luminescent AIE molecules. For instance, Luo et al.[96] carried out a one-pot synthesis of highly luminescent Au(I)-thiolate complexes with strong AIE properties. In light of this, *in situ*-generated Au(0) nuclei induced controlled aggregation of Au(I)-thiolate complexes to form Au(0)@Au(I)-thiolate core−shell structures, with a strong fluorescence quantum yield of 15%. Similarly, thiolated Ag NCs with significant AIE properties were also synthesized. Zheng et al.[97] reported that in simple boiling water, thiol-stabilized Ag NCs showed a characteristic absorption profile, large Stokes shift, and strong fluorescence emission at 686 nm. A highly luminescent thiol-stabilized Cu NCs with AIE properties and a quantum yield of 14.1% was also successfully prepared. After solvent evaporation, the solid Cu NCs showed an increased quantum yield (16.6%), a large Stokes shift (295 nm), and a long fluorescence lifetime (150.6 μs), which are consistent with AIE properties[98]. Aggregation/assembly has also been used to induce AIE properties. A study reported that silk fibroin-protected fluorescent Cu NCs showed unique AIE characteristics with the assistance of sulfide ions in aqueous solution[99]. In another study, a research group achieved AIE-featured Au NCs through Ag doping to engineer the size/structure and aggregation states of the Au(I)−thiolate motifs in the NC shell[100]. Various substances that can induce AIE features have been explored. A study reported that GSH-capped Cu NCs displayed AIE characteristics, rapidly aggregated in the presence of Al^{3+} ions, and induced enhanced red emission[101]. Such significant clues drive the achievement of AIE properties in bio-inspired metal NCs for biomedical applications.

3.6. *Biological effect*

Biomolecules play a crucial role in biological functions and physiological processes due to their intrinsic sequence, conformation, bioactivity, and interaction of bio-interface, which are widely applied in the design and fabrication of nanoparticles in the field of medicine. The conformation and structure of biomolecules are the key factors for biological applications. Thus, metal NCs could be rationally grafted by customized biomolecules to achieve their extensive bioactivities, excellent biocompatibility, and physiological response. Theoretically, biomolecular ligands localized on the surface of metal NCs rapidly bind to biological targets and affect the subsequent biological process. It is worthy of note that the collaborative implication of biomolecular templates of encapsulated metal NCs and subsequent biological efficacy remains to be verified. Recent advances in biological studies have shown that biomolecules in physiological milieu extensively

involve bio-responsiveness, specific recognition, catalysis, and signal transduction, such as aptamer recognition, antigen−antibody, RNA−DNA, protein−DNA, hormone−receptor, enzyme−substrate, and streptomycin−avidin interactions. Nevertheless, the multi-level conformation and biological functions of biomolecules (proteins, peptides, and DNA) are violently destructive during the synthesis of metal NCs. As a typical case, the catalytic kinetics of bovine pancreatic α-chymotrypsin (CHT) conjugated Ag NCs were delayed by approximately 2−3-fold due to dynamic changes in the stiffness of Ag NCs upon CHT attachment[102]. In another example, human transferrin-stabilized Au_{22-33} NCs with strong fluorescence emission (695 nm) in the near-infrared region were successfully applied to cell imaging in A549 cells. Antibody-induced aggregation experiments confirmed that the protein preserved its ability to target corresponding receptors[103]. As a drug complex, biomolecule stabilized metal NCs not only retained biological activities by utilizing surface ligands, but also had a visualized tracing for pharmaceutical effect[104]. Based on the customization strategy, Liu's group[105] designed a tripeptide that contained a TrxR1-inhibiting peptide segment, which was subsequently employed to prepare Au NCs. The resultant Au NCs could stably bind to TrxR1 and inhibit its biological activity, significantly causing the production of higher levels of reactive oxygen species (ROS) and consequently cell apoptosis. In addition to protein/peptide-coated metal NCs, artificially tailored DNA sequences can be designed as new DNA templates for the preparation of metal NCs through DNA molecular recognition sequence and ability to react with metal NCs, indicating great promise in bio-labeling, imaging, and therapeutics[106−108]. Therefore, the biological implication of biomolecules for the synthesis and functionalization of metal NCs should be thoroughly investigated.

4. Therapeutic applications of bio-inspired metal NCs

As a hybrid organic−inorganic system, the combination of metal NCs with characteristic biomolecules/cells provides real-time monitoring and combined therapy for disease treatment and analysis. In combination with therapeutic modalities and bio-nanotechnology, the synthesis and functionalization of metal NCs with well-defined molecular structures have been intensively carried out. Imaging-guided and functional properties have inspired material scientists to fabricate bio-inspired metal NCs for the synchronization of visualization and treatment with the ultimate goal of real-time monitoring, bio-responsiveness, enhanced therapeutic effect, and controllable efficacy[109]. In light of this, the principles and resultant properties of bio-inspired metal NCs favor their therapeutic applications. As demonstrated by *in vitro* and *in vivo* studies, we discuss the versatility of bio-inspired metal NCs to investigate their therapeutic effect.

4.1. *Bioprobes*

Owing to the complexity of biological systems, organs, and biological barriers, it is meaningful to develop specific biological probes with high safety for dynamic analysis. The critical points of bioprobe technology depend on two aspects: the transmit component with strong fluorescence and excellent stability and the specific recognition of the target. On the one hand, the rich library of biomolecules closely associated with numerous biological processes and targets act as functional domains and growth

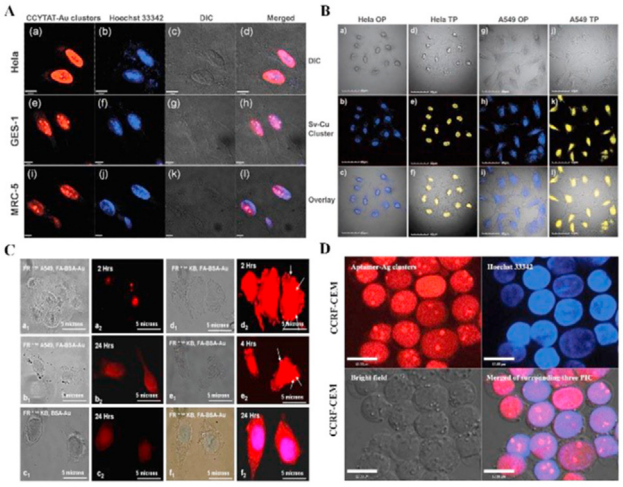

Figure 2 (A) Confocal image of cellular staining of Hela, GES-1, and MRC-5 cells with CCYTAT-Au NCs and Hoechst 33342. The CCYTAT-Au NCs exhibited red emission (λ_{em} = 640 nm), and Hoechst 33342 emitting blue emission (λ_{em} = 440 nm) was used as a reference for nuclear staining. Scale bar = 40 μm. Reprinted with permission from Ref. 46. Copyright © 2012, the Royal Society of Chemistry. (B) One- and two-photon confocal images of the Sv-Cu clusters for HeLa and A549 cells. Blue and yellow represent one- and two-photon emission, respectively. Scale bar = 40 μm. Reprinted with permission from Ref. 91. Copyright © 2013, the Royal Society of Chemistry. (C) Fluorescent microscopic images showing the interaction of FA-BSA-Au NCs with different types of cell lines. Scale bar = 5 μm. Reprinted with permission from Ref. 123. Copyright © 2009, Institute of Physics Publishing Ltd. (D) Fluorescent images of aptamer-Ag NCs and Hoechst 33342 in live CCRF-CEM cells were observed by confocal microscopy. The red emission of Ag NCs and the blue emission of Hoechst 33342 at 561 nm (top left) and 488 nm excitation (top right), respectively. The bright field imaging of cells (lower left). Merged image of the above three images (lower right). Scale bar = 5 μm. Reprinted with permission from Ref. 128. Copyright © 2011, the Royal Society of Chemistry.

scaffolds, showing synergistic efficacy for multimodal bioimaging and targeting due to tunable fluorescence emission, matchless biocompatibility, and variable bioactivities[110,111]. A sub-2 nm metal core fabricated with a biomolecule shell can penetrate biological barriers and achieve cell or organelle localization with renal clearance ability[69,112]. On the other hand, atomically precise metal NCs with good photostability, strong luminescence with microsecond luminescence lifetime, large Stokes shift (>200 nm), and NIR emission are beneficial for bioimaging. Specifically, NIR-II imaging at 1100−1700 nm possesses deep penetration and high resolution in biological tissues, which is particularly useful for medical diagnosis related to blood vessels[113]. With the ease of integration with other imaging elements and imaging technologies, such complementary features could be exploited for *in vitro* and *in vivo* fluorescent bioimaging. The following section discusses imaging performance and design principles.

4.1.1. *In vitro imaging*

In general, the functionalization of biomolecules and the inherent fluorescence of metal NCs result in synergistic properties, which facilitate subcellular localization and cell imaging. For the first time, Yu et al.[114] fabricated fluorescent Ag NCs for efficient

cellular imaging by using three short peptides extracted from nucleolin, which indicates that nucleolin is a very useful candidate for the preparation of biocompatible Ag NCs and other argyrophilic proteins. Our previous study showed that silk fibroin-derived peptide directed Ag NCs for cell imaging in murine preosteoblast MC3T3-E1 cells. The result of the study confirmed a simple approach for the easy fabrication of Ag NCs based on characteristic peptides and that fluorescent staining of cell nuclei could be possibly ascribed to transport by endocytosis due to the ultrasmall size and positive charge of peptide−Ag NCs[115]. Furthermore, the images of fluorescent Cu NCs encapsulated by CLEDNN, an artificial peptide, indicated a strong blue fluorescence in the cell membrane of HeLa cells and cytoplasmic area, whereas the fluorescence in the cell nucleus was very weak[116]. Combining cell-penetrating peptide with NPs is an effective strategy to penetrate the cell membrane. As shown in Fig. 2A, Wang et al.[46] designed a bifunctional peptide (CCYTAT) containing one HIV-1 TAT domain that penetrated and targeted cell nuclei and another domain capable of biomineralizing and capturing Au NCs. The synthesized Au_{25} NCs specifically targeted the nucleus of the three kinds of cell lines (Hela, GES-1, and MRC-5) with the red fluorescence emission. In addition, Cu_{14} NCs were facilely prepared with a bifunctional peptide that contains cluster formation sequence (CCY) and nuclear localization sequence (NLS: PKKKRKVG), suggesting an outstanding capability of one- and two-photon imaging for cell nuclei of both HeLa and A549 cells (Fig. 2B)[91]. By comparison, the uptake and the fluorescence images of blue-green, yellow, and red-emitting GSH-Ag NCs were observed in the cytoplasm, through endocytosis, and not in the nucleus of epithelial lung cancer A549 cells[117]. Unlike GSH-Ag NCs, blue-emitting GSH-Cu NCs were observed primarily in the nuclear membranes of three cancerous cells (Hela, MDAMB-231, and A549 cells) with high biocompatibility and imaging stability[118]. In addition, various biomolecular drugs have been used for the synthesis of metal NCs in the bioimaging fields. Insulin-Au NCs have demonstrated the feasibility of using two-photon red fluorescence imaging and CT, offering innovative and supplementary methods, compared with conventional isotope[124] I-insulin and anti-insulin antibody conjugated with a chemiluminescent enzyme. It is worth noting that fluorescent insulin-directed Au NCs have excellent biocompatibility and the ability to regulate glucose levels[119]. For the first time, our group reported aprotinin-encapsulated Au NCs with desirable red fluorescence, which indicates dynamic subcellular targeting of the cytoplasm and nucleus in HeLa cells. Interestingly, Au NCs contributed to endosomal escape and entry into the nucleus as Au clusters encapsulated by aprotinin collectively favored the penetration of the cytomembrane, escape of the endolysosomal pathway, and passage through the nuclear pore into the nucleus[120]. Apart from peptide−metal NCs, non-toxic and bright protein-protected metal NCs are feasible for cellular imaging. Human transferrin protected Au_{22-33} NCs with a high fluorescence emission in the near-infrared region (λ_{em} = 695 nm), suggesting the uptake of the iron-loaded fluorescent proteins into the cytoplasm of A549 cells for cell imaging and targeting. Notably, antibody-induced agglomeration confirmed no alteration in protein activity and the ability to target receptors[121]. In another study, the conjugation of folic acid with BSA-Au_{25} NCs favored significant endocytosis in receptor-targeted cancer detection of FR-positive oral squamous cell carcinoma (KB) and breast adenocarcinoma MCF-7 cells. By comparison, FA-conjugated BSA-Au_{25} clusters were found to be internalized at significantly higher concentrations than the negative control cell lines. Moreover, a large number of red-emitting FA-BSA-Au_{25} NCs conjugates were attached to the cell membrane of FR-positive KB cells as early as after 2 h of incubation. With longer incubation times of 4 and 24 h, the concentration of aggregated metal NCs on the cell membrane reduced with an increase in fluorescence at the intracellular region, and the metal NCs were completely internalized in the cytosol (Fig. 2C)[122]. In another case, BSA-Au_{38} NCs conjugated with folic acid showed cell imaging effect in oral carcinoma KB cells through folic acid-mediated endocytosis and no significant luminescence was observed in L929 cells containing very few folic acid receptors[123]. Besides, a myriad of protein-encapsulated Au NCs were exploited for cell imaging. For instance, ovalbumin (OVA), *N*-acryloxysuccinimide, and folic acid as the fluorescent component, linker, and targeting ligand, respectively, were successfully applied for specific staining and imaging of HeLa cells[124]. Bovine pancreatic ribonuclease A-encapsulated Au NCs integrated with vitamin B12 was used for simultaneous targeting and imaging of Caco-2 cell lines[45]. DNA-templated Ag NCs in aqueous solution are attracting increasing attention in a wide range of cellular imaging applications, owing to their ultrasmall size, excellent photostability, the principle of complementary base pairing, and good biocompatibility. Generally, DNA-Ag NCs tend to appear most prominently in the nucleus[125]. For instance, Choi et al.[126] engineered a wide range of emission and multicolor staining of Ag NCs for intracellular applications through tailored oligonucleotide scaffolds. The Ag NCs selectively stained the nuclei of fixed NIH3T3 cells with green emission, exhibiting excellent photostability under both one- and two-photon excitation. Furthermore, Ag_3 and Ag_4 NCs synthesized by artificially modified Sgc8c DNA aptamers that are capable of red emission when excited by light, were used to specifically target the nucleus of CCRF-CEM live cells. However, a trypan blue exclusion assay showed that the Ag NCs exhibited great cytotoxicity towards the CCRF-CEM cells, whereas the Sgc8c molecules were not cytotoxic to the cells (Fig. 2D)[127]. As for *in vivo* bioimaging, the NIR imaging probes are usually favorable due to decreased optical scattering at this wavelength range, deep penetration of photons, and increased resolution in biological tissues.

4.1.2. *In vivo bioimaging*

A safe bioprobe with real-time monitoring, effective targeting, long blood circulation, effective renal clearance, good biocompatibility over organic fluorophores and QDs, significantly contribute to the prognosis, diagnosis, and treatment of diseases[128,129]. As a typical instance, Zhou et al.[130] demonstrated that near-IR-emitting GSH-Au NCs with a diameter of approximately 2 nm could be stabilized during blood circulation and cleared out of the body through kidney filtration, thus validating high feasibility for *in vivo* imaging application. In another study, Liu et al.[131] produced luminescent GSH-Au NCs, with a diameter of ~2.5 nm, that behaved like small dye molecules (IRDye 800CW) and enabled prolonged tumor retention time, faster normal tissue clearance, improved tumor targeting, enhanced permeability, and retention effect (Fig. 3A). Moreover, folic acid-conjugated GSH-Au NCs were adopted for dual-mode fluorescence/X-ray computed tomography imaging of gastric cancer MGC-803 cells[132]. NIR absorbance is highly advantageous for optimal penetration of light into animal tissues. By using *in vivo* fluorescence imaging, Yu et al.[29] employed renal-clearable NIR-emitting Au NCs to noninvasively detect kidney dysfunction, the dysfunctional stages, and the adaptive function in a mouse model

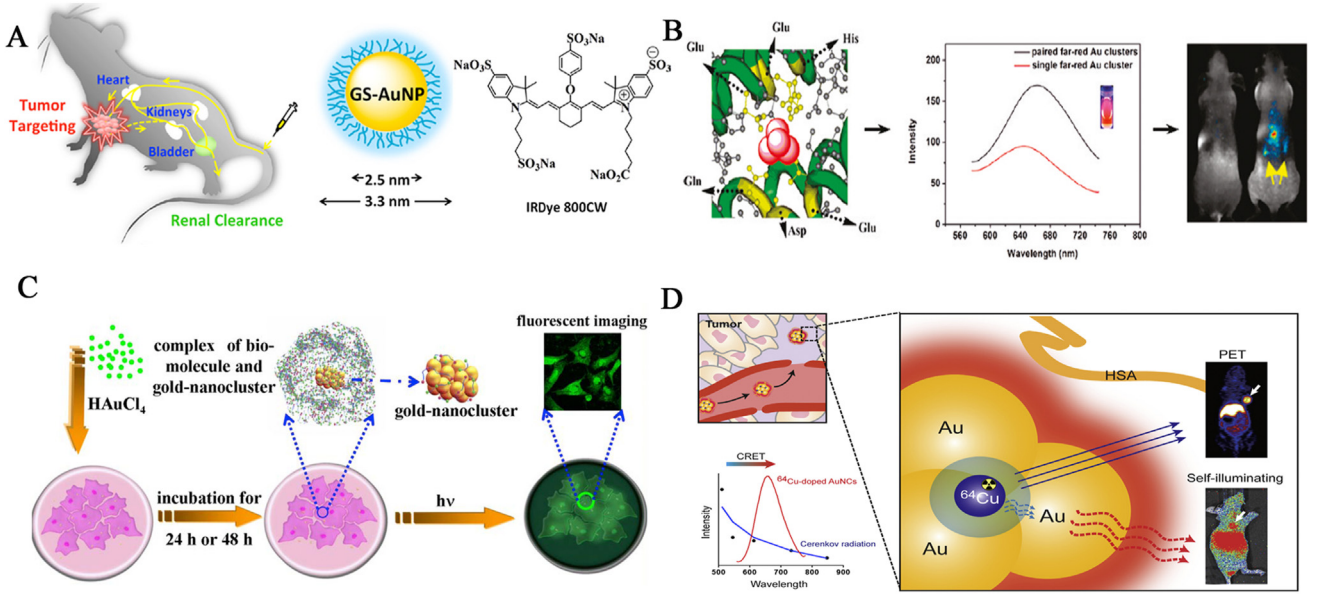

Figure 3 (A) Schematic illustration of passive tumor targeting by GSH-Au NCs and IR Dye 800CW. *In vivo* NIR fluorescence images of MCF-7 tumor-bearing mice intravenously injected with GSH-Au NCs and IRDye 800CW collected at 0.5, 3, and 12 h post-injection. The tumor areas are indicated with arrows. Organ distribution of GSH-Au NCs and IRDye 800CW. Labels: 1, tumor; 2, liver; 3, lung; 4, spleen; 5, heart; 6, kidney (left); 7, kidney (right). Reprinted with permission from Ref. 131. Copyright © 2013, American Chemical Society. (B) A schematic representative of controllable assembly of paired Au NCs within ferritin nanoreactor for *in vivo* kidney targeting and imaging. Reprinted with permission from Ref. 43. Copyright © 2011, American Chemical Society. (C) Schematic illustration of the complex of Ag^{+} with GSH to form the biosynthesized Ag NCs for *in vivo* bioimaging study in xenograft tumor nude mice models of cervical carcinoma. Reprinted with permission from Ref. 138. Copyright © 2014, Nature Publishing Group. (D) Self-illuminating ^{64}Cu-doped Au NCs for *in vivo* synergistic dual-modality positron emission tomography (PET) and self-illuminating NIR imaging. PET radionuclide ^{64}Cu plays dual roles as the positron-emitting radionuclide (tracer) for PET imaging as well as the energy donor to excite Au NCs. The Au NCs as the energy acceptor was adopted for self-illuminating NIR fluorescence imaging. Reprinted with permission from Ref. 141. Copyright © 2014, Elsevier.

of unilateral obstructive nephropathy. Regarding the use of protein-Au NCs, Wu et al.[133] reported that ultrasmall NIR BSA-Au NCs as novel contrast imaging agents allowed continuous *in vivo* and *ex vivo* tumor imaging and high accumulation of ultrasmall NIR Au NCs in MDA-MB-45 and HeLa tumor xenograft models due to enhanced permeability and retention effects. Notably, the fluorescent imaging signal of the tail vein in living organisms could be spectrally discriminated from the background with a maximum emission wavelength at approximately 710 nm. For other Au NCs, Liu et al.[134] proposed folic acid-modified trypsin-Au NCs with near-infrared fluorescence and high specific affinity to FR-positive tumors and carried out an *in vivo* study of the dynamic behavior and targeting ability. As shown in Fig. 3B, Sun and colleagues[43] employed an assembly strategy by combining two Au NCs at the ferroxidase active sites of ferritin heavy chain. The resultant Au-Ft nanostructures not only retained the intrinsic fluorescence properties of noble metal NCs and the excellent biocompatibility and organ-specific targeting ability of native ferritin, but also gained enhanced intensity, a red shift, and tunable emissions due to the coupling interaction between the paired Au NCs. Specific cells as potent scaffolds can be explored for the synthesis of metallic nanomaterials[135,136]. As a typical example, *in situ* biosynthesized fluorescent Au NCs were produced by Au(III) reduction upon entry into the cytoplasm and ultimately concentrated around the nucleoli of cells of various cancer cells (HepG2, human hepatocarcinoma, K562, and leukemia cell lines) with specific fluorescent self-bio-marking. It is worth mentioning that this reaction takes place in cancerous cells, with human embryo liver cells (L02) as controls[137]. Moreover, as evidenced in Fig. 3C, the spontaneous self-generation of Ag NCs with high near-infrared fluorescence emission was successfully established by the intracellular reduction of innocuous silver salts inside cancer cells, which demonstrated precise and selective imaging in both *ex vivo* experiments and *in vivo* imaging of subcutaneous cervical carcinoma xenografted model in nude mice[138]. An integrated multimodal strategy that is capable of generating stable and effective biomolecule-noble metal complexes with controllable size and desirable fluorescence emission is promising for *in vitro* and *in vivo* imaging. As shown in Fig. 3D, using a chelator-free doping method, Hu et al.[139] prepared non-toxic, self-illuminating ^{64}Cu-doped HSA-Au NCs for dual-modality positron emission tomography (PET) and NIR fluorescence imaging in a U87MG glioblastoma xenograft model through Cerenkov resonance energy transfer. PET radionuclide ^{64}Cu played dual roles as the energy donor and the PET imaging source, and Au NCs acted as the energy acceptor for NIR fluorescence imaging.

4.2. *Radiosensitizer*

Radiotherapy is a part of the treatment regime for patients with an unresectable disease to improve survival after tumor surgical removal. In bio-inspired metal NC systems, an ideal radiosensitizer requires enhanced radiotherapy, high tumor-targeting capability, excellent biocompatibility, and efficient renal clearance to avoid potential side effects to patients (Fig. 4A)[140]. To some

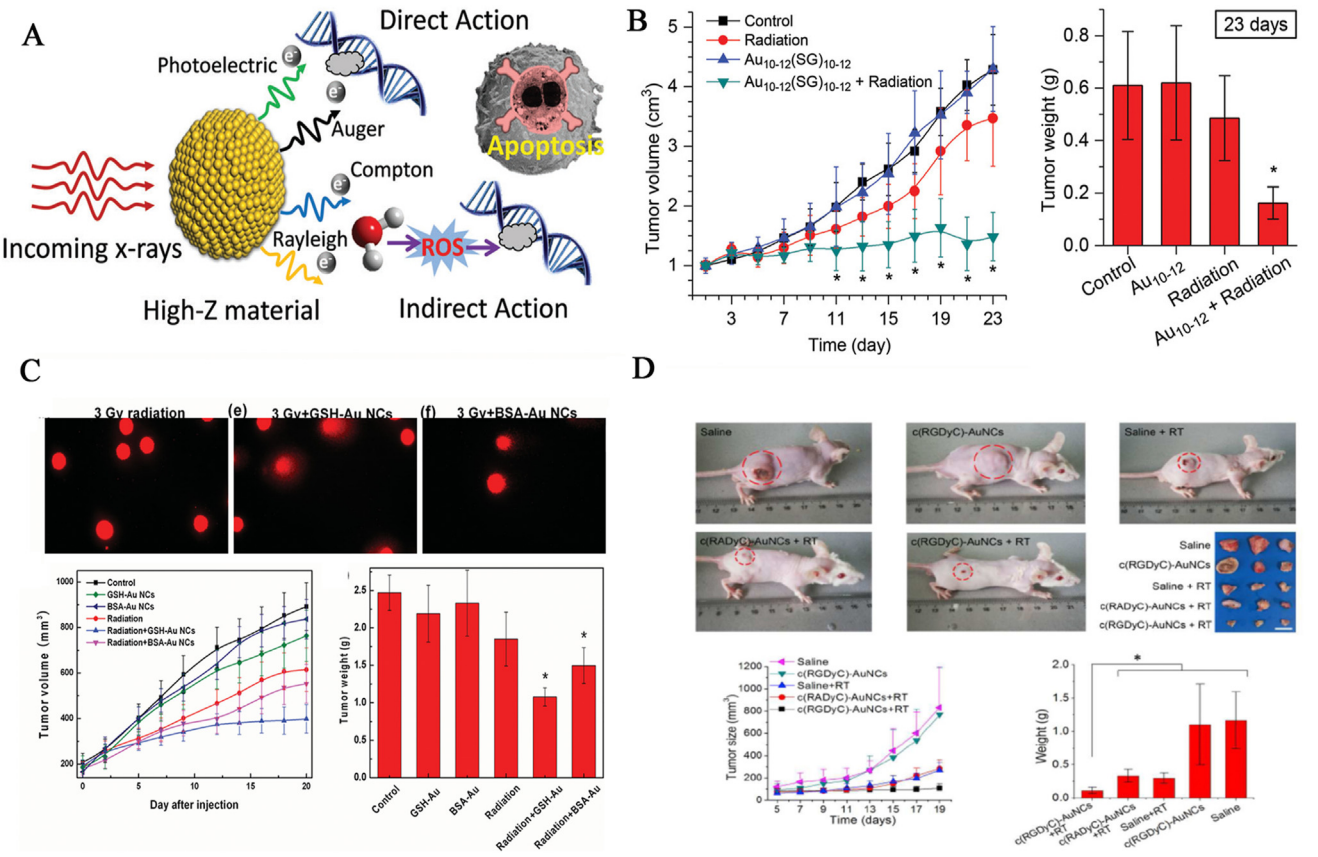

Figure 4 (A) Schematic illustration of interactions of X-rays with high-Z materials and the corresponding direct and indirect effects on cancer cells. Reprinted with permission from Ref. 140. Copyright © 2017, the Royal Society of Chemistry. (B) Schematic illustration of the structure of $Au_{10}(SG)_{10}$ nanomolecule for high radiotherapy. Reprinted with permission from Ref. 143. Copyright © 2014, John Wiley & Sons, Inc. (C) Schematic illustration of the structures of GSH-Au_{25} NCs and BSA-Au_{25} NCs nanomolecules for high radiotherapy. Reprinted with permission from Ref. 145. Copyright © 2014, John Wiley & Sons, Inc. (D) Schematic representation of c(RGDyC)-Au NCs, which exhibited selectively enhanced targeting and accumulation of $\alpha v\beta 3$ integrin-positive cancer cells with red/NIR fluorescence emission. Reprinted with permission from Ref. 146. Copyright © 2017, Elsevier.

extent, large Au NPs as radiosensitizers cause high *in vivo* toxicity due to the obvious accumulation of the NPs in the liver and spleen, inducing gene regulation and liver necrosis[141]. To avoid such toxic side effects, ultrasmall metal NCs with high-Z atoms, which can effectively enhance photoelectric absorption and secondary electron yield, should be used to facilitate high tumor specificity, clearance by the RES organs, and efficient urinary excretion[140,142]. Thus, a series of Au NCs with distinct compositions were productively utilized as novel radiotherapy sensitizers with therapeutically enhanced efficiency due to the variable atomic number of gold and good biocompatibility. As a typical example, Zhang et al.[143] reported a new class of GSH-Au NCs with a well-defined molecular formula of $Au_{10-12}(SG)_{10-12}$, which was validated as an ideal sensitizer for radiotherapy with enhanced safety and significant efficacy. It is worth mentioning that the highly biocompatible GSH shell exposed on the surface of the nanomolecule allowed the NCs to escape RES absorption and facilitated selective targeting capability, ultrahigh tumor uptake, and efficient renal clearance, significantly contributing to enhanced radiotherapy (Fig. 4B). Similarly, another study reported GSH-coated $Au_{29-43}(SG)_{27-37}$ NCs as excellent radiosensitizers with high tumor uptake within 24 h post injection, strong enhancement for radiotherapy, and negligible damage to normal tissues[144]. Furthermore, with naturally occurring biomolecules as stabilized ligands, GSH-Au_{25} NCs and BSA-Au_{25} NCs displayed strong radiotherapy enhancement because of the inherent enhancement of radiotherapy by gold atoms and good biocompatibility derived from the GSH or BSA shell. In addition, GSH-Au_{25} NCs caused a discernible decrease in tumor volume and weight with enhanced radiotherapy, were efficiently cleared by the kidney after treatment, and exhibited reduced potential side effects. However, the larger BSA-Au_{25} NCs were not efficiently removed by the kidney, which caused liver damage (Fig. 4C)[145]. As shown in Fig. 4D, Liang and coworkers[146] employed cyclic arginine-glycine-aspartic acid [c(RGDyC)] peptide to prepare c(RGDyC)-Au NCs, which selectively enhanced the targeting and accumulation of $\alpha v\beta 3$ integrin-positive cancer cells with red/NIR fluorescence emission. Notably, the radiosensitizer significantly enhanced the efficacy of radiotherapy, which was 1.51- and 1.25-fold larger than those obtained by non-targeted c(RADyC)-Au NCs and clinically used radiosensitizer CMNa. In addition, CCYKFR-Au_{25} NCs after endocytosis presented highly efficient targeting and accumulation in the mitochondria, significantly introducing a burst of mito ROS for severe DNA damage and cancer cell death when irradiated by 4 Gy X-rays[147]. The bio-inspired strategy could be universally expanded to develop new

metal NCs with improved radiosensitization for personal treatment, where the physicochemical properties of metal NCs largely determine their capability.

4.3. *Photosensitizers*

Phototherapy, namely photothermal therapy (PTT) and PDT, is a form of medical treatment whereby specific wavelengths of light are used to treat diseases, such as cancers and peripheral infections, to rehabilitate the body and ameliorate depression[148,149]. Upon illumination, a photosensitizer is capable of transferring the absorbed photon energy to surrounding oxygen molecules or heat from optical energy. This leads to the production of ROS, such as free radicals or singlet oxygen, which prompt specific cell death and tissue destruction without any obvious damage to the adjacent healthy cells in the dark[150]. As for PDT, the well-defined metal NCs should encourage energy transfer to molecular oxygen to facilitate the formation of $^1O_2$ in disease treatment. As a general strategy, the covalent coupling of folic acid and polyethylene glycol (PEG) on the surface of GSH-Au NCs was carried out, followed by the loading of the photosensitizer Ce6 within the PEG networks and its attachment to the Au NC surface. Unlike the free Ce6, *in vitro* studies showed that the nanoprobe exhibited enhanced cellular uptake and satisfactory efficacy in MGC-803 cells (Fig. 5A)[151]. As shown in Fig. 5B, another new nanoformula, SiO_2-Ce6-Au NCs, showed a remarkably improved fluorescence imaging-guided photodynamic therapeutic efficacy, compared with the free Ce6. The improved efficacy was attributed to prominent features such as high loading of Ce6, significantly enhanced cellular uptake of Ce6, no nonspecific release of Ce6 during its circulation, and subcellular characterization[152]. Khlebtsov et al.[57] fabricated Au-BSA-antiSAIgG-PS complex by conjugating BSA-Au NCs with human anti-staphylococcal immunoglobulin (antiSAIgG) and Ce6, which significantly inactivated bacteria *S. aureus* under 660 nm light irradiation. To achieve synergistic efficacy, Li et al.[153] designed BSA-encapsulated Pt NCs (BSA-Pt NCs) as a source of O_2 and further conjugated them with mesoporous silica nanospheres and photosensitizer methylene blue to develop a nanoformula for improved therapeutic outcomes against hypoxic tumors. In the formulation, the nanocomposites exhibited low cytotoxicity, and O_2 was continuously produced through the decomposition of H_2O_2 in a tumor microenvironment, owing to the outstanding biocompatibility features of BSA and the enhanced catalytic activity of Pt NCs. More importantly, exploring the molecular basis of metal NCs for $^1O_2$ photosensitization can be used to control their therapeutic performance. To this end, it is suggested that the optical gap of $Au_{25}(SR)_{18}$ NCs (~1.3 eV), which is larger than the energy of $^1O_2$ (0.97 eV), allows for efficient energy transfer to $^3O_2$[154]. In light of this, Agrachev et al.[155] investigated the

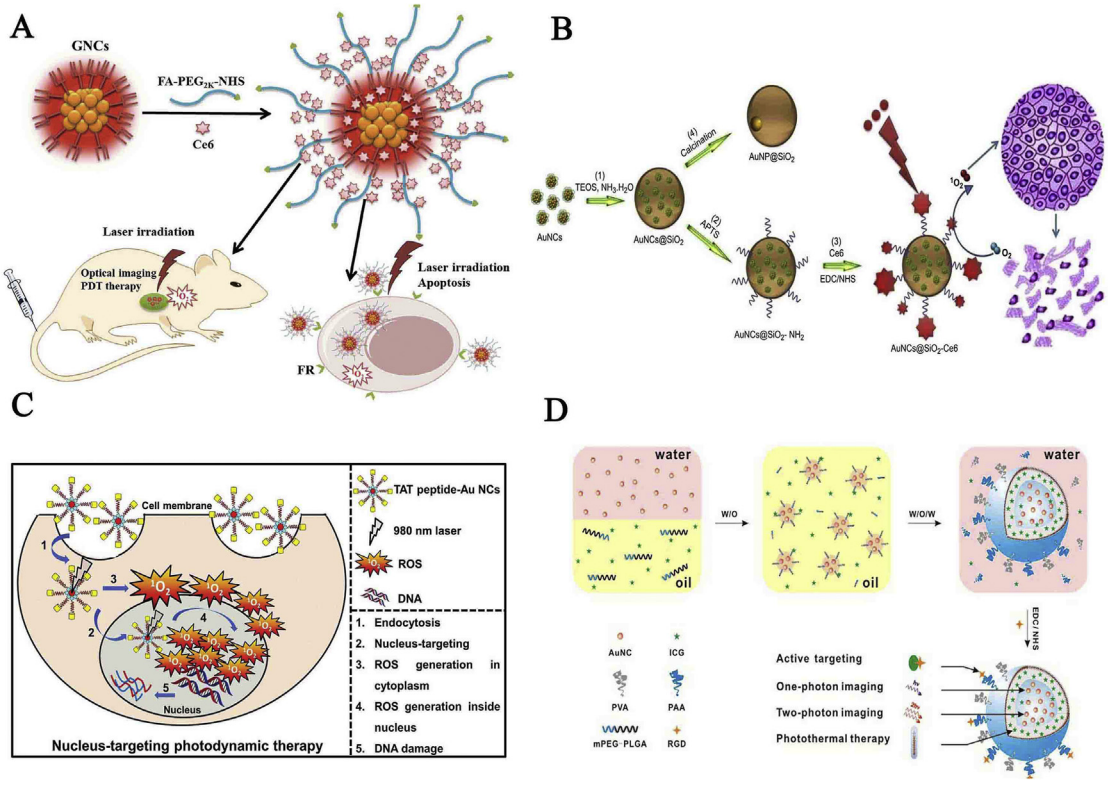

Figure 5 (A) Schematic illustration of the preparation of Au NCs-based nanoprobes and their photodynamic therapy (PDT) applications *in vitro* and *in vivo*. Reprinted with permission from Ref. 151. Copyright © 2015, John Wiley & Sons, Inc. (B) Illustration of the synthesis of Ce6-conjugated silica-coated Au NCs for PDT therapy. Reprinted with permission from Ref. 152. Copyright © 2013, Elsevier. (C) Diagram representing the nucleus-targeting TAT peptide-Au NCs for PDT. Cell viability, R generation, and DNA fragmentation assay were evaluated by using HeLa cells. Reprinted with permission from Ref. 156. Copyright © 2015, John Wiley & Sons, Inc. (D) Schematic illustration of the formation of RGD-conjugated Au NCs-ICG-mPEG-PLGA nanocapsules. Temperature change curves and infrared thermal results of different suspensions over a period of 5 min with exposure on the 808 nm light. Reprinted with permission from Ref. 158. Copyright © 2016, the Royal Society of Chemistry.

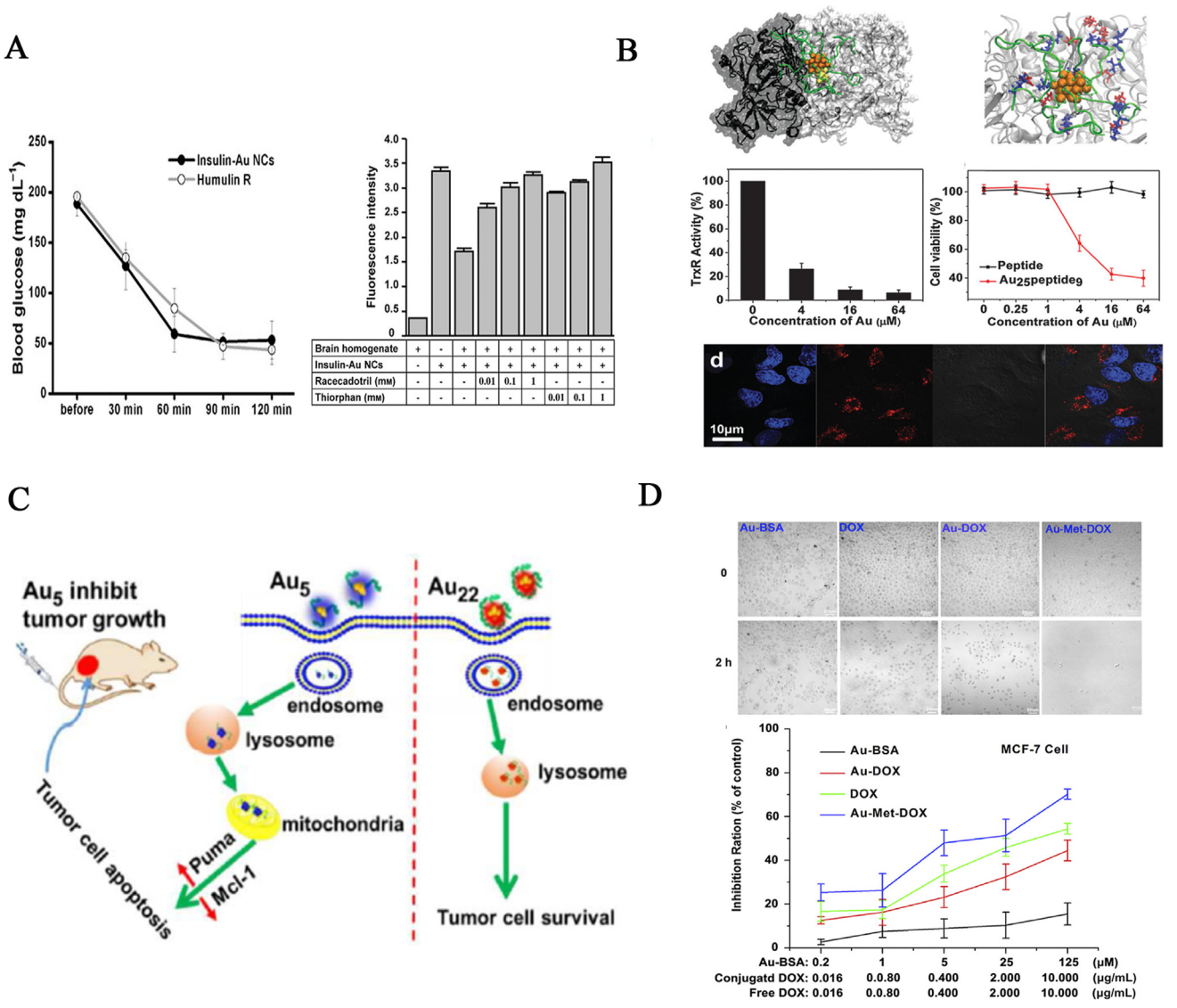

Figure 6 (A) Blood glucose *versus* elapsed time of treatment with insulin-Au NCs and humulin R in Wistar rats. Fluorescence quenching of insulin-Au NCs by brain homogenate, which is inhibited by racecadotril and thiorphan. Reprinted with permission from Ref. 119. Copyright © 2011, John Wiley & Sons Ltd. (B) The structure of the gold cluster-TrxR1 complex. TrxR1 activity is suppressed in a dose-dependent manner by serial doses of $Au_{25}Peptide_9$. Scale bar = 10 μm. Reprinted with permission from Ref. 105. Copyright © 2014, American Chemical Society. (C) Au_5 but not Au_{22} suppressed tumor growth *via* mitochondria target and triggered cell apoptosis *in vitro*/*in vivo*. Reprinted with permission from Ref. 167. Copyright © 2018, American Chemical Society. (D) Schematic representation of the assessment of the antitumor capability of Au-BSA, DOX, Au-DOX, and Au-Met-DOX in MCF-7 tumor cells. Reprinted with permission from Ref. 170. Copyright © 2012, Elsevier.

efficiency of singlet-oxygen photosensitizers by using a series of atomically precise $Au_{24}M(SR)_{18}$ clusters, with different R groups and doping metal atoms M. The study showed that the metal clusters yielded results similar to those designed with a well-known reference photosensitizer. In addition, TAT peptide-Au NCs exhibited a significant nucleus-targeting and sensitized the formation of singlet oxygen for NIR-light activated PDT (Fig. 5C)[156]. As for PTT, GSH-platinum NCs showed effective bioimaging of HeLa and HepG2 cells and efficient treatment of cancers upon infrared irradiation[157]. In another strategy, BSA-Au NCs and indocyanine green (ICG) were loaded with mPEG-PLGA to fabricate hybrid nanocapsules through a double emulsion process. The hybrid nanocapsules achieved one-photon/two-photon fluorescence imaging and photothermal ablation of the tumor (Fig. 5D)[158]. *In situ* biosynthesized platinum NCs by cancerous cells could be readily achieved in a biological milieu, emitting bright fluorescence at 460 nm, and this could be further utilized to facilitate excellent cancer-cell-killing effect when combined with porphyrin derivatives for photothermal treatment[51]. Thus, concerning the photoactivatable conversion efficiency, investigating the size and structure of metal NCs is very necessary for the future design of novel photosensitizers.

4.4. *Drug conjugates*

Bio-inspired metal NCs consisting of metal complexes and biomolecular drugs hold great promise in the pharmaceutical industry. However, the related research is still at an early stage.

Metal compounds have been used as therapeutic agents for centuries, and the records can date back to 2500 BC in China and ancient Arab. So far, auranofin, a gold compound that was approved for the treatment of rheumatoid arthritis, and *cis*-platinum complexes have been used for the treatment of cancer. Meanwhile, apart from antibodies and enzymes as biomolecular drugs, approximately 140 peptide therapeutics are currently being evaluated in clinical trials[34,159]. Thus, utilizing surface modification and tailorability of biopharmaceutical biomolecules, a bioinspired strategy could be used for the design of metal NCs for potent treatment, target specificity, and enhanced therapeutic efficacy with minimized toxicity[160]. As shown in Fig. 6A, a newly developed fluorescent insulin-Au NCs retained the blood glucose-reducing effect of insulin. Racecadotril and thiorphan, which are able to inhibit the insulin-degrading enzyme, also prevented the degradation of insulin-Au NCs[119]. In another typical case, Wang et al.[56] conjugated fluorescent BSA-Au NCs with Herceptin (Her-Au NCs) for synergistic nucleus imaging and cancer therapy. The resultant Her-Au NCs was able to escape the endolysosomal pathway and enter the nucleus of cancer cells, which enhanced the therapeutic efficacy of Herceptin in ErbB2 over-expressing breast cancer cells and tumor tissue. Thioredoxin (Trx) and trx reductase (TrxR) as redox-active proteins have been implicated in multiple cellular events, including growth promotion, apoptosis, and cytoprotection and the activity of TrxR1 in the cytoplasm can be significantly suppressed by the specific functional peptide[161]. Based on this principle, Liu and coworkers[105] designed tridecapeptide-templated Au_{25} NCs, which significantly suppressed TrxR1 activity in the cytoplasm and induced the up-regulation of activated PARP in a dose-dependent manner. Thus, the characterization and the regulation of biological properties of Au NCs will help to determine the various functional ligands that can be conjugated with Au NCs for tumor therapy (Fig. 6B). Li and colleagues[162] evaluated the therapeutic effect of peptide-templated Au_{25} NCs on chronic lymphocytic leukemia cells. MEC-1 cell apoptosis occurred in a dose-dependent manner, correlating with the uptake of metal NCs in cells and the amount of ROS. In another case, Zhao and coworkers[163] reported that wheat germ agglutinin-protected Au_{25} NCs conjugated with HIV-1 TAT peptide entered the cell nucleus, resulting in the production of ROS, mitochondrial damage, and cell apoptosis. Regarding the binding specificity of Au NCs, An et al.[164] introduced molecular dynamics simulation to study the structure of tridecapeptide-coated Au_{25} NCs and their interactions with TrxR1. Biased corona peptide motion, spreading, and cooperation between peptide extensions were facilitated by bacterial stimulus-driven approach and adhesion mechanisms mediated by cilia as well as a typical hydrophobic interaction with TrxR1. The results indicated that the peptide-coated Au NCs acted as an adept thioredoxin mimic for an array of auxiliary structural components that were capable of enhancing interactions with the target protein. Molecular dynamic simulation was introduced to rationally design and screen serial peptide-Au NCs by targeting specific proteins in "lock and key" molecular interaction mode. The synthesis of peptide-Au NCs and the suppression of glutathione peroxidase-1 (GPx-1) activity were verified by theoretical simulation that specifically recognized and bound to the specific domain of GPx-1 with high affinity in buffer and cells, respectively[165]. Xia et al.[166] reported a Pt NCs assembly (Pt-NA) composed of assembled Pt NCs and incorporating a pH-sensitive polymer and hepatocellular carcinoma (HCC)-targeting peptide. These Pt NAs could inhibit the proliferation of disseminated HCC-initiating cancer stem-like cells by targeting the DNA. Interestingly, Zhai et al.[167] reported two Au clusters with precisely controlled molecular size ($Au_5Peptide_3$ and $Au_{22}Peptide_{10}$) showing different antitumor effects. Au_5, but not Au_{22}, suppressed tumor growth by targeting the mitochondria, and this was a breakthrough in the nanomedical field. This discovery provided a robust approach for turning on/off the medical properties of NPs by atomically controlling their sizes (Fig. 6C). Chemotherapeutic drugs can easily be conjugated with the functional group of metal MCs. For example, the conjugation of doxorubicin (DOX) with folic acid-conjugated BSA-Au NCs (DOX-FA-Au NCs) simultaneously displayed selective tumor-targeting efficacy and enhanced antitumor activity[168]. For instance, fluorescent Au NCs were conjugated with a cisplatin prodrug (Pt) and FA to form Pt-FA-Au NCs, which generated strong fluorescence signals in 4T1 tumor-bearing nude mouse model and caused significant inhibition of the growth and lung metastasis of orthotopically implanted 4T1 breast tumors[169]. Similarly, a nanocomposite was prepared by combining BSA-Au NCs, conjugated with methionine and functionalized with a near-infrared fluorescent dye (MPA), and a prodrug (DOX). The nanocomposite exhibited *in vitro* and *in vivo* tumor-targeting imaging and a better antitumor activity than the prodrug (Fig. 6D)[170]. Thus, the combination of biomolecular drugs with metal clusters provides a flexible platform for combined therapeutics.

4.5. *Nanovaccines*

A vaccine is a class of biological agents conferring active acquired immunity to a particular disease, including tumor-related proteins or peptides, tumor antigens, and cell lysates[171,172]. The introduction of nanotechnology for improved solubility, permeability, stability, and pharmacokinetics overcomes the general shortcomings of traditional subunit vaccines, such as the poor and short-lived immunogenicity, inefficient uptake by professional antigen-presenting cells, as well as fast degradation by metabolic enzymes[173–175]. Generally, un-methylated cytosine-phosphate-guanine (CpG) dinucleotide, or the CpG motif, commonly presents in natural viral and bacterial DNA, can strongly stimulate the immune system to recognize and trigger both innate and adaptive immune responses of the mammalian immune system, and it has been used for the design of novel vaccines[176,177]. To potentiate the action of vaccine, Qu's group[178] appended CpG motifs to the DNA template to develop functionalized CpG-Ag NCs as efficient immunostimulatory agents with high biocompatibility, increased CpG stability against nuclease degradation, enhanced CpG-uptake by TLR9-positive cells, and remarkable immunostimulatory activity (Fig. 7A). Similarly, Tao et al.[179] prepared OVA-CpG oligodeoxynucleotides (ODNs)-templated Au NCs-based vaccines through a facile one-pot synthesis, and they performed not only as an imaging agent, but also as a vaccine that generated high and significantly enhanced immunostimulatory activity through dual-delivery of protein antigen and CpG ODNs, compared with the original antigen. As shown in Fig. 7B, OVA-derived peptide (SIINFEKL) was capable of inducing strong $CD8^+$ cytolytic T cell response. Tao et al.[180] fabricated CpG-OVA peptide-Au NC conjugates that simultaneously delivered peptide antigens and CpG ODNs into the same APCs, which improved cross-presentation and induced strong immunostimulatory reactions both *in vitro* and *in vivo*, especially by increasing strong $CD8^+$ cytolytic T cell response.

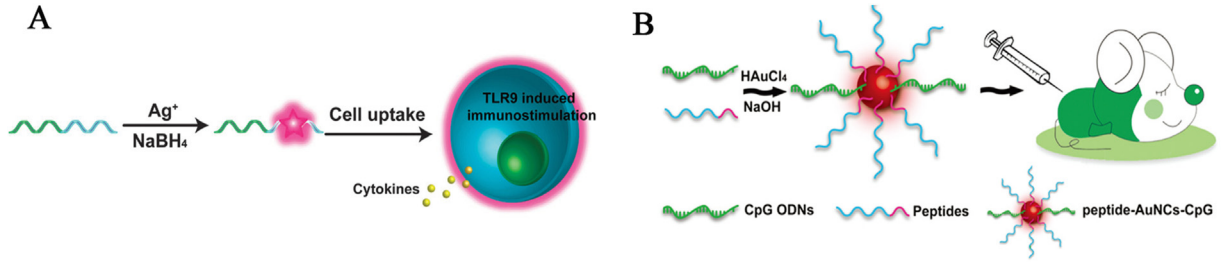

Figure 7 (A) Schematic illustration of the synthesis of CpG-Ag NCs, their immunostimulatory effect, and the comparison of cytokine release from RAW264.7 cells stimulated by CpG-Ag NCs. Reprinted with permission from Ref. 178. Copyright © 2013, the Royal Society of Chemistry. (B) General scheme for the synthesis of peptide-Au NC-CpG conjugates to induce an immune response. Reprinted with permission from Ref. 180. Copyright © 2015, the Royal Society of Chemistry.

4.6. *Nanocarriers*

Spurred by the development of micro-nanotechnology, micro-nanocarrier systems have been increasingly used for drug delivery[181,182]. Generally, an ideal nanocarrier is expected to carry NPs with high tumor specificity without toxic side effects, achieve efficient urinary excretion, and bypass clearance by the RES organs, such as the liver and spleen. Meanwhile, the successful delivery of gene, protein, and some other molecules is a novel therapeutic technique to correct or repair defective symptoms responsible for diseases, largely depending on the development of appropriate carriers that can rapidly and efficiently deliver target material into cells with minimized toxicity[183−185]. However, there are only a few clinically approved nanocarriers that can incorporate molecules to selectively bind and target cancer cells. For controllable delivery and release, the rich surface chemistry of biomolecule-encapsulated metal NCs can be tuned to meet the need for drug and gene delivery. As shown in Fig. 8A, Li and colleagues[186] developed a novel multifunctional probe comprising a cell-specific internalization aptamer, fluorescent Ag NCs, and therapeutic siRNA into one entity to achieve cell targeting and simultaneous noninvasive imaging, excellent fluorescent stability, tunable fluorescence emission wavelength of Ag NCs from DNA template sequences, along with enhanced stability of siRNA. In another case, TAT peptide-Au NCs showed ∼80% gene transfection efficiency of DNA delivery cargoes in HeLa cells, which was nearly 3.2-fold higher than that of the most commonly adopted LP2000 liposome gene carrier. It has also demonstrated excellent photostability and appreciable biocompatibility in HeLa cells as well as in *in vivo* zebrafish model system[156]. Subsequently, a combinatorial therapy was reported using cationic BSA Au−Ag NC composite NPs loaded with pDNA. Along with the delivery and tracking of therapeutic suicide genes, the composite NPs initiated a therapeutic response cascade by converting prodrug 5-FC to 5-FU and causing the production of ROS, which triggered apoptosis-mediated cell death[187]. To construct a responsive property in the nanocarrier system, BSA-templated Cd NCs conjugated with hyaluronic acid (HA) formed a pH-responsive, tumor-targeting theranostic nanocarrier with low cytotoxicity and a continuous release profile for the delivery of doxorubicin (DOX), a model anticancer drug. This study showed that the nanocarrier obtained a DOX encapsulation efficiency of up to approximately 75.6% and the release of DOX at pH 5.3, with less than 26% of DOX released at pH 7.4 within the same 24 h period (Fig. 8B)[188]. As an emerging nanocarrier, Lei and coworkers[189] further reported that GSH-Au NCs-assisted siRNA delivery of NGF (GNC-siRNA) was validated for potent NGF gene silencing, and it effectively inhibited tumor progression without adverse effects in three pancreatic tumor models, including a subcutaneous model, orthotopic model, and patient-derived xenograft model. The GNC−siRNA complex afforded higher loading capacity of siRNA with increased stability of siRNA in the serum, prolonged the circulation lifetime of siRNA, and enhanced the cellular uptake and tumor accumulation of siRNA, most likely due to the smaller size and larger specific surface area of GNCs (Fig. 8C).

4.7. *Antimicrobial agents*

Prompted by the critical challenge of bacterial contamination and antibiotic resistance, considerable effort has been devoted to the discovery and development of new types of antibacterial agents[190,191]. With the unique advantages of real-time monitoring and ultrafine size, the integration of antimicrobial components into the architecture of bio-inspired metal NCs could serve as a new, highly efficient antimicrobial alternative for the inhibition of the growth of detrimental bacteria, especially antibiotic-resistant bacteria. As shown in Fig. 9A, tunable luminescent emitting GSH-Ag NCs with well-defined size and composition, $Ag_{16}(SG)_9$, and $Ag_9(SG)_6$, were fabricated *via* size/structure-focusing processes. With real-time monitoring of the dynamic antimicrobial process, compared with $Ag_9(SG)_6$, the highly red luminescent $Ag_{16}(SG)_9$ generated a high concentration of intracellular ROS and acquired superior antimicrobial properties against *Pseudomonas aeruginosa,* a multidrug-resistant bacteria[69]. Meanwhile, it has been shown that the un-dissociated Ag^+-R NCs armed with abundant Ag^+ ions on the surface were highly active in bacterial killing, compared with their larger counterpart, Ag NPs. Subsequently, Xie's group[192] synthesized ultrasmall GSH-protected Ag^+-rich NCs, which showed higher antimicrobial activities against both Gram-negative and Gram-positive bacteria than the reference NCs, GSH-Ag^0-R NCs. The GSH-Ag^+-R NCs had the same size and surface ligands as the GSH-Ag^0-R NCs, but different oxidation states of silver (Fig. 9B). In addition, the formation of Ag complexes with different structures and stabilities are regarded as key factors that can modulate their antibacterial activities. For example, it has been reported that the sequence-dependent Ag NCs emitting blue, yellow, and red fluorescent emission yielded different antibacterial activities against Gram-positive and Gram-negative bacteria. Significantly, the yellow and red emitters afforded a comparable activity to that of silver nitrate, whereas the blue emitters yielded poor antibacterial activity[193]. Besides silver NCs, Au NCs could kill both Gram-positive and Gram-negative bacteria. This wide-spectrum antimicrobial activity is attributed to the ultrasmall size of Au NCs,

which allows better interaction with bacteria[194]. Alloying is an efficient chemistry to diversify the properties of metal NPs. Zheng et al.[195] developed a full spectrum of alloy metal NCs, $Au_xAg_{25-x}(MHA)_{18}$ (MHA = 6-mercaptohexanoic acid) with $x = 0-25$, and they observed a U-shape antimicrobial behavior instead of the common increasing trend. An accessible method to establish antimicrobial properties is to combine antimicrobial enzymes or antibiotic peptides with metal NCs. As shown in Fig. 9C, Yang's group integrated bactericides with various metal NCs as one entity to achieve a higher antibacterial effect. Meanwhile, bacitracin-Ag NCs, Au NCs, and Cu NCs emitted cyan, yellow, and red fluorescence, respectively. Significantly, bacitracin-Ag NCs exhibited a robust bacteria-killing effect, compared with other NCs, owing to the marked damage to the bacterial membrane[196]. In another study, lysozymes, which are capable of hydrolyzing the cell walls of pathogenic bacteria, were used for the synthesis of lysozyme-Au NCs. The NCs effectively inhibited the cell growth of notorious antibiotic-resistant bacteria, including pan-drug-resistant *Acinetobacter baumannii* and vancomycin-resistant *Enterococcus faecalis*[197]. Similarly, Miao and colleagues[198] synthesized papain-functionalized Cu NCs in aqueous solution together with red fluorescence at 620 nm and a quantum yield of 14.3%. Notably, with Cu NCs plus H_2O_2 rather than Cu NCs or H_2O_2 alone, Cu NCs converted H_2O_2 to •OH and exhibited an outstanding antibacterial activity against *S. aureus* and *Escherichia coli.* Furthermore, the results of *in vivo* experiment on mice with infected wound showed that no erythema and edema was formed in the treated mice. In another example, two distinctive bactericides were integrated into one entity for improved efficacy. As shown in Fig. 9D, Zheng et al.[199] designed an efficient antimicrobial hybrid formed by conjugating Ag NCs with daptomycin to achieve the improved antibacterial activity. The hybrid system inherited the intrinsic properties of both bactericides with an enhanced synergistic performance that could effectively damage the bacterial membrane and present improved bacteria-killing efficiency over the physically mixed daptomycin and Ag NCs (D + Ag NCs). The aforementioned examples confirmed the efficacy of bio-inspired NCs for various bacterial.

4.8. *Nanozymes*

The use of biocatalysis for therapeutic applications is on the verge of significant growth. In essence, enzyme mimetics mimic some properties and functions of an enzyme, producing robust and better catalytic performance[200,201]. Along with the introduction of various types of enzyme mimetics and the search for efficient modulators of catalysis at different rates and selectivity, the development of metal NCs increasingly provides biomimetic catalysts that are capable of competing with catalytic proficiency

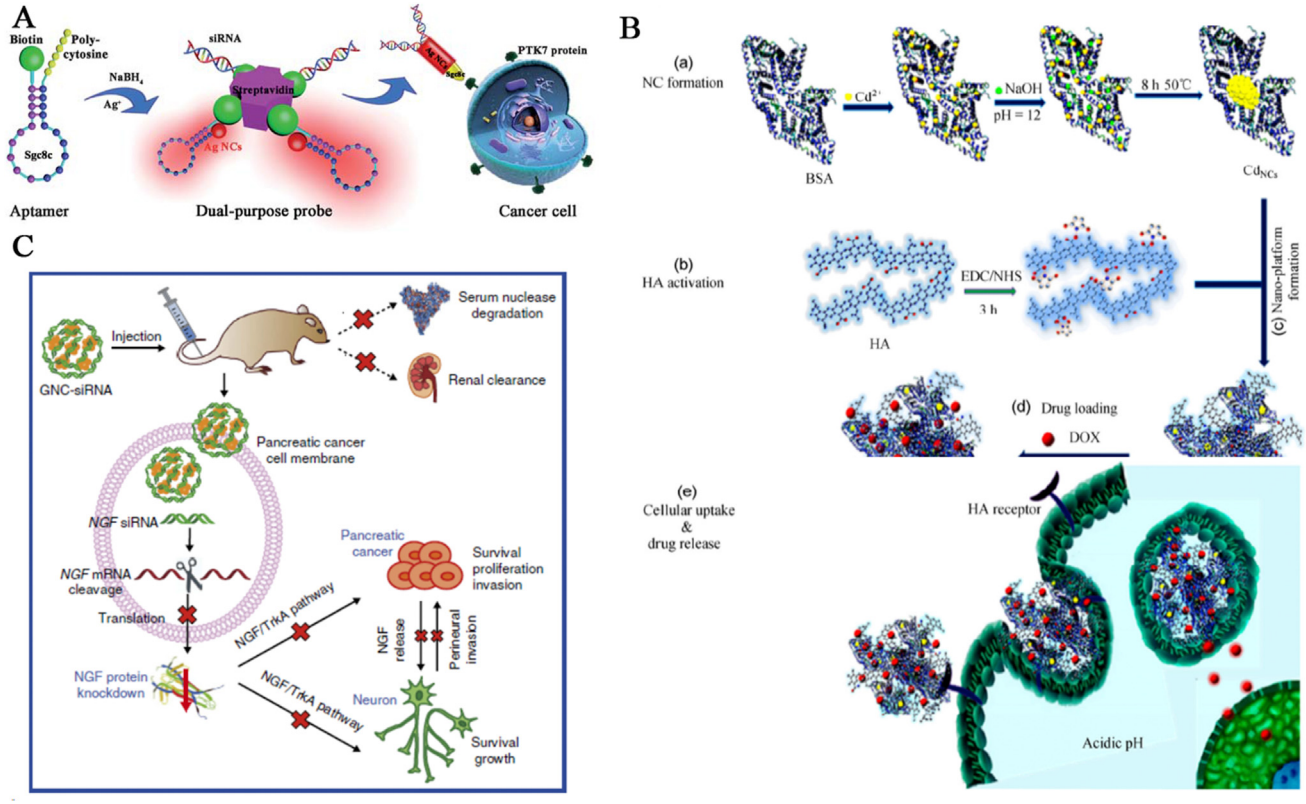

Figure 8 (A) Schematic representation of aptamer-functionalized Ag NCs-assisted siRNA delivery and tracking for type-specific cells. Reprinted with permission from Ref. 186. Copyright © 2013, the Royal Society of Chemistry. (B) Schematic illustration of the synthesis of Cd NCs, doxorubicin (DOX) loading into the HA-Cd NC nanocarrier (DOX-HA-Cd NCs), and HA receptor-directed targeted drug delivery. Reprinted with permission from Ref. 188. Copyright © 2016, Tsinghua University Press. (C) Schematic illustration of the delivery mechanism of Au NCs-siRNA complex for NGF silencing and pancreatic cancer therapy. The Au NCs-siRNA complex protected the NGF siRNA from serum nuclease degradation and renal clearance, thus enhancing the accumulation of NGF siRNA in tumor cells. Reprinted with permission from Ref. 189. Copyright © 2017, Nature Publishing Group.

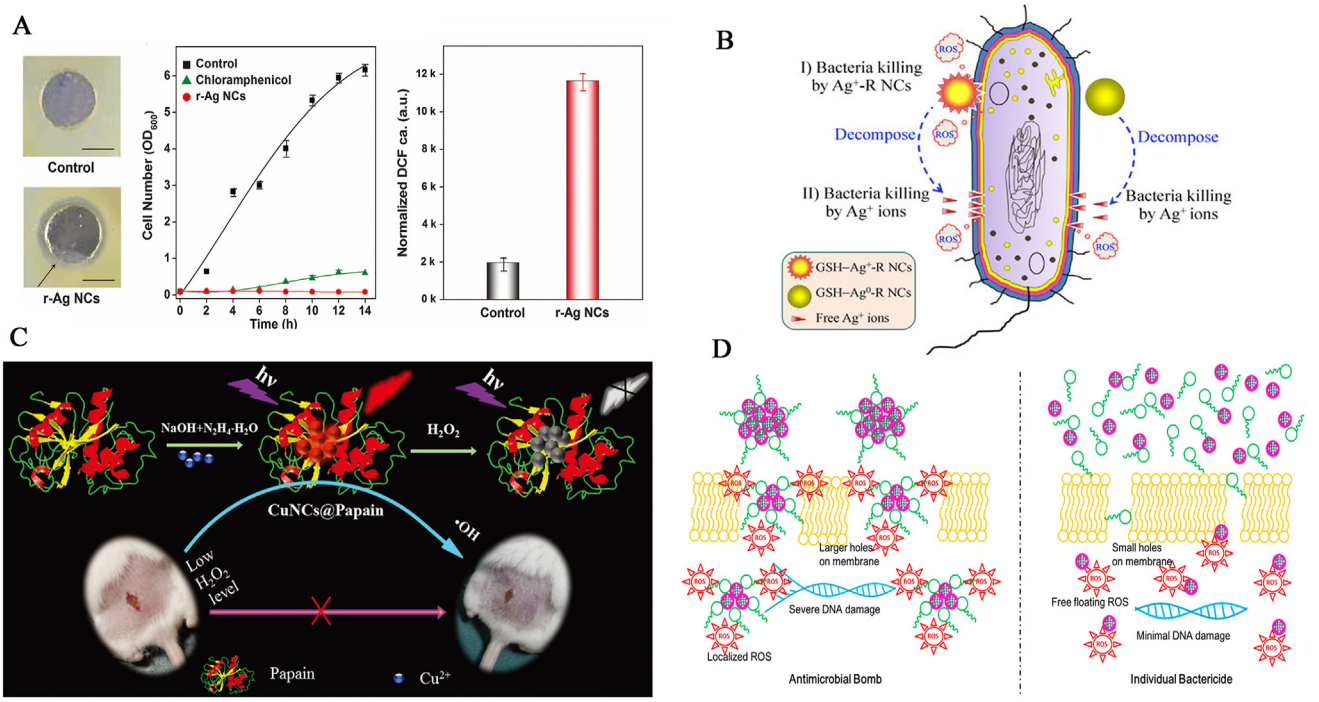

Figure 9 (A) Evaluation of the antibacterial activity of $Ag_{16}(SG)_9$. Reprinted with permission from Ref. 69. Copyright © 2013, Nature Publishing Group. (B) Schematic illustration of possible antimicrobial mechanisms of GSH-Ag^+-R NCs and GSH-Ag^0-R NCs. Reprinted with permission from Ref. 192. Copyright © 2014, Tsinghua University Press. (C) Schematic diagram of synthesized water-soluble Cu NCs interacting with H_2O_2 and their application in avoiding disinfection. Reprinted with permission from Ref. 196. Copyright © 2020, American Chemical Society. (D) The chemically integrated D-Ag NCs showed improved antibacterial effect over the physically mixed daptomycin and Ag NCs (D + Ag NCs). Reprinted with permission from Ref. 199. Copyright © 2016, American Chemical Society.

of enzymes in the fields of bionics, biosensing, and biomedical sciences[202–204]. Typically, BSA-Au NCs presented a high peroxidase-like activity, which was used for the colorimetric detection of as low as 2.0×10^{-8} mol/L H_2O_2. In comparison with the other kinds of NPs that are peroxidase mimetics, including Fe_3O_4, FeS, or graphene oxide, a study showed that BSA-Au NCs were more competent for biocatalysis because of their ultrasmall size, good stability, and high biocompatibility in aqueous solution. Furthermore, it was reported that the optimal pH for catalytic activity was 3.0[205]. Afterwards, a higher peroxidase-like activity at a near-neutral pH was observed with BSA-Cu NCs. The peroxidase-like catalysis of Cu NCs exhibited Michaelis−Menten kinetics that was comparable to that of horseradish peroxidase. In comparison to natural enzymes, Cu NCs offer several advantages as a mimic peroxidase due to ease of preparation, low cost, as well as high stability and activity under harsh conditions (Fig. 10A)[206]. As for Pt NCs, BSA-Pt NCs with an average diameter of 2.0 nm consisted of 57% Pt^0 and 43% Pt^{2+}, which maintained highly peroxidase-like activity with Km values of 0.119 and 41.8 mmol/L towards 3,3,5,5-tetramethylbenzidine (TMB) and H_2O_2[207]. In addition, a new type of ultrasmall Pt NCs, with yeast extract as the reductant and stabilizer, possessed attractive peroxidase-mimicking property. The NCs efficiently catalyzed the oxidation of TMB in the presence of H_2O_2[208]. Generally, biomolecule-assisted metal NCs exhibit peroxidase-like activity. Hu et al.[209] fabricated an enzyme-mimetic nanoprobe based on folate receptor-targeting Au NCs for simultaneous and mutually complementary peroxidase and fluorescent staining of MCF-7 and HepG2 tumor cell slices. The nanoprobe significantly improved the accuracy and specificity of the cancer diagnosis without false-positive and false-negative results. Furthermore, catalytic labels that amplify the detection of the duplex generated between the analyzing primer and the target DNA have been used in specific bio-applications. Based on this concept, Zhao et al.[210] utilized enzyme-mimetic GSH-Au NCs conjugated on the outer layer antibody to catalyze the decomposition of hydrogen peroxide to form a sandwiched antibody-antigen-antibody structure, allowing a naked-eye readout ultrasensitive and visually quantitative determination of ultra-trace target molecules. This type of nanosensor was validated by the determination of various ultra-trace analytes including protein avidin, a breast cancer antigen, thyroid hormone, and methamphetamine (Fig. 10B). More recently, it has been proposed that platinum nanomaterials exhibit four kinds of enzyme-like activities, including superoxide dismutase, catalase, oxidase, and peroxidase activities[211–213]. Lysozyme-Pt NCs exhibit the maximal fluorescence at 434 nm with a quantum yield of 0.08 and an intrinsic oxidase-like activity, catalyzing O_2 oxidation of organic substrates through a four-electron reduction process. Compared with larger Pt NPs, Pt NCs exhibited considerably greater catalytic activity in the O_2-mediated oxidation of 2,2′-azino-bis(3-ethylbenzothiazoline-6-sulphonic acid), TMB, and dopamine, compared with larger Pt NPs[41]. The introduction of an enzyme modulator plays a crucial role in the regulation of the activity of metal NC-based enzyme mimetics. Intriguingly, graphene oxide (GO) was used as an enzyme modulator to regulate the peroxidase-like activity of lysozyme-Au NCs. Dramatic improvement in catalytic activity was observed with a gradual increase in GO concentration. The synergistic catalyst, the GO-Au NCs hybrid (GA), exhibited excellent peroxidase-like activity over a broad pH range, even at neutral pH, by simply adsorbing

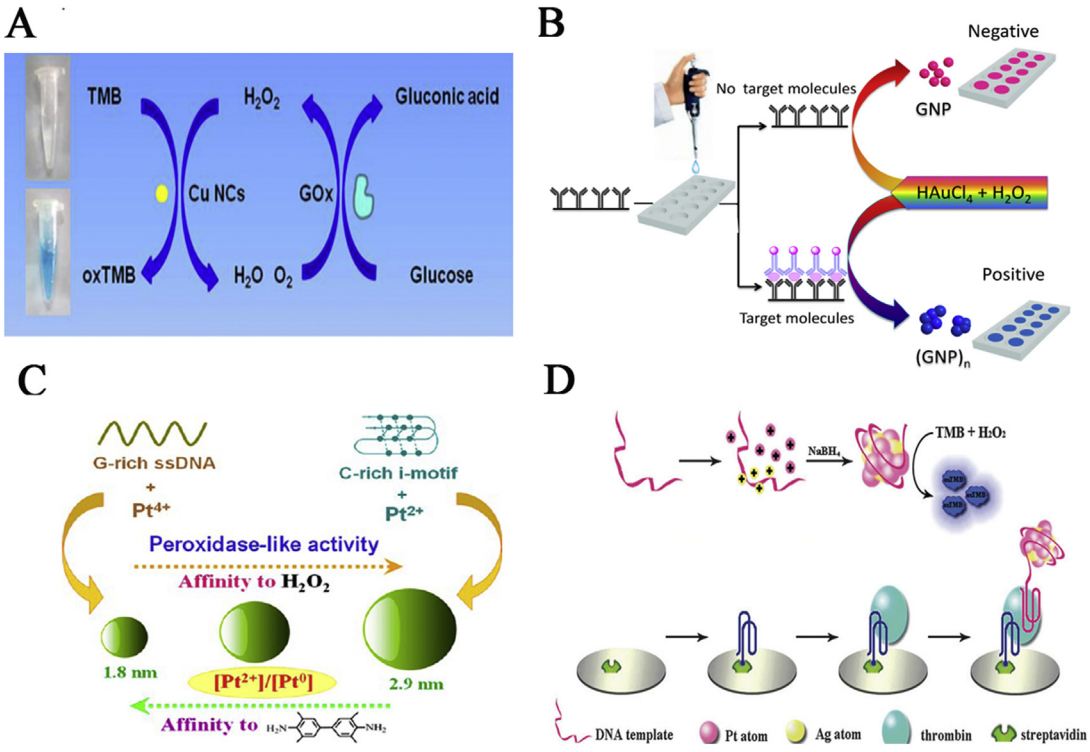

Figure 10 (A) Schematic representation of copper nanoclusters as peroxidase mimetics and their catalysis application to H_2O_2. Reprinted with permission from Ref. 206. Copyright © 2013, Elsevier. (B) Schematic representation of the plasmonic nanosensor. In sandwich structure, the target molecule is anchored to the substrate by capture antibodies and recognized by other antibodies labeled with Au NCs. Reprinted with permission from Ref. 210. Copyright © 2015, American Chemical Society. (C) G-/C-rich oligonucleotides-directed Pt enzymes with a size distribution of 1.7−2.9 nm mimic high peroxidase activity. Reprinted with permission from Ref. 217. Copyright © 2014, American Chemical Society. (D) Schematic illustration of the synthesis of DNA-Ag/Pt NC and colorimetric detection for human thrombin. Reprinted with permission from Ref. 216 Copyright © 2014, the Royal Society of Chemistry.

lysozyme-Au NCs on GO surface through electrostatic interaction[214]. In another strategy, the production of metal NC-based enzymes to modulate physicochemical properties could easily be achieved by programming DNA sequences. It has been reported that a series of DNA oligonucleotides-templated Pt enzymes, with a size distribution of 1.7−2.9 nm, showed variable peroxidase-mimic activities. When the average size increased from 1.8 to 2.9 nm, the proportion of Pt^0 species increased while that of Pt^{2+} decreased. The K_m value for H_2O_2 decreased by three folds, whereas that for TMB increased by two folds (Fig. 10C)[215]. Moreover, as shown in Fig. 10D, DNA-templated Ag/Pt bimetallic NCs (DNA-Ag/Pt NCs) revealed intrinsic highly efficient peroxidase-like catalytic activity. Owing to the ultrasmall size and the synergistic effect of Ag in bimetallic NCs, the peroxidase-like activity of DNA-Ag/Pt NCs was significantly higher than that of DNA-Pt NCs at an equivalent dose of Pt content[216]. Further efforts could be made to explore metal NCs with various enzyme-like and enzyme-modulating activities to mimic and control enzymatic activities, respectively.

5. Cytotoxicity and biodistribution

To accelerate potential clinical applications, safety concerns on the formulation of bio-inspired metal NCs should be systemically evaluated in the early stage. The investigation of the cytotoxicity, biodistribution, and pharmacokinetic behavior profiles of bio-inspired nanomaterials lays an underlying foundation for targeted anticancer therapies without side effects. Biomolecules, such as human serum albumin (HSA), facilitate efficient cellular internalization, prolonged blood circulation time, intensive tissue penetration depth, and favorable pharmacokinetics and biodistribution. However, the function and ultimate efficiency of most therapeutic NPs remain unsatisfactory for clinical application, mainly because of the unpredictability of nanomaterial−biology interactions, poor biodegradability, and large size. Consequently, the interplay of nanomaterials with biological systems can predict the toxicological effects of nanomaterials *in vivo*[217−219]. To explain this, BSA-Cu NC treatment affected the viability of C2C12 cells in a dose-dependent manner, decreased the mitochondrial membrane potential, and elicited apoptosis, along with an increase in the protein expression ratio of BAX/BCL-2 and caspase-3/9 activity. It was also reported that Cu NCs induced morphological atrophy in primary muscle cells and mouse gastrocnemius muscle cells[220]. Moreover, chiral metal NCs play a role in various applications of sensing, biomedicine, and catalysis, owing to their unique physical and chemical properties[221,222]. Zhang and colleagues[223] reported that the D-GSH-Ag NCs showed higher toxicity than L-GSH-Ag NCs in both human gastric mucous epithelial GES-1 and human gastric cancer MGC-803 cells (Fig. 11A). For comparison, Zhang et al.[224] fabricated both L-GSH-Au and D-GSH-Au NCs to induce ROS generation and activate integrated cytotoxic effects that involved DNA damage, mitochondrial depolarization, cell cycle arrest, and apoptosis-mediated death. Notably, the D-GSH-Au NCs were more toxic than the L-GSH-Au NCs to both MGC-803 and GES-1 cells. For a comprehensive understanding, a systematic comparison of the

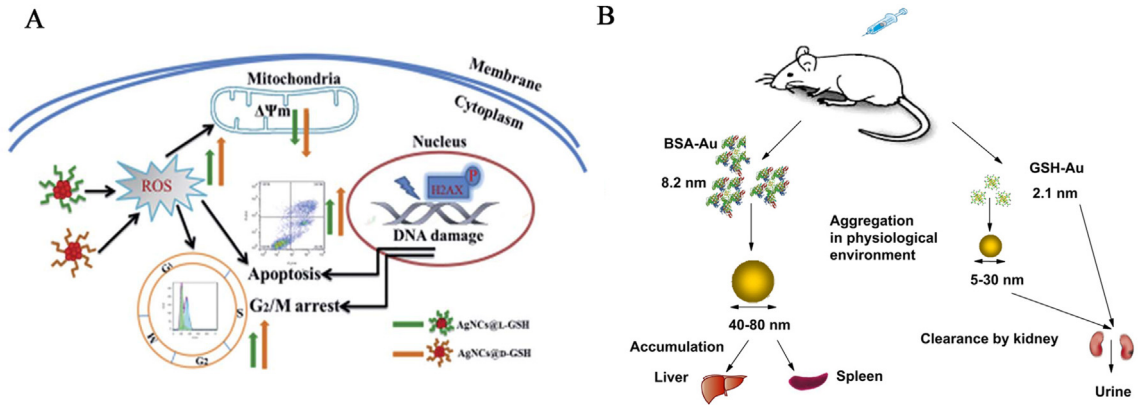

Figure 11 (A) Schematic illustration of the synthesis and cytotoxicity of L-GSH-Ag NCs and D-GSH-Ag NCs and the potential molecular mechanism. Reprinted with permission from Ref. 223. Copyright © 2014, the Royal Society of Chemistry. (B) Schematic representation of the biodistribution and renal clearance of GSH- and BSA-protected Au_{25} NCs. Reprinted with permission from Ref. 225. Copyright © 2012, Elsevier.

in vivo renal clearance, biodistribution, and toxicity responses of the BSA-Au NCs and GSH-Au NCs for 24 h and 28 days, respectively, were determined. The toxicity responses for GSH-Au NCs were eliminated after 28 days; nevertheless, BSA-Au NCs accumulated in the liver and spleen and caused an irreparable toxicity response. The biodistribution results revealed that 94% of gold was metabolized for the GSH-Au NCs, but only less than 5% of gold was metabolized for the BSA-Au NCs after 28 days. The renal clearance of BSA-Au NCs was low, and only 1% and 5% of gold was cleared after 24 h and 28 days, respectively; however, the GSH-Au NCs had more efficient renal clearance with 36% and 94% of gold cleared, respectively (Fig. 11B)[225]. Moreover, Wang et al.[226] evaluated the *in vivo* biodistribution, excretion, toxicity, and tumor uptake of GSH-protected Au NCs of a similar hydrodynamic size but with three different surface charges (positive, negative, and neutral) over 90 days. The results revealed that the surface charge significantly influenced pharmacokinetics, particularly renal excretion and accumulation in the kidney, liver, spleen, and testis. Negatively charged Au NCs generally showed lower excretion and higher tumor uptake, indicating a possibility for NC-based therapeutics, whereas positively charged metal NCs caused transient side effects on the peripheral blood system.

6. Conclusions and perspectives

As an emerging class of fluorescent nanomaterials with hybrid metal core-ligand shell structures and combinational properties, bio-inspired metal NCs provides synergistic properties for imaging-guided combined therapy, such as ultrafine size, tunable fluorescence, real-time monitoring, biocompatibility, bio-responsiveness, and enhanced therapeutic efficacy. In the current review, we provide a state-of-the-art overview of bio-inspired metal NCs comprising various biomolecules (protein, peptide, and DNA) and cells as functional scaffolds, with particular emphasis on well-established strategies and design rationale for specific purposes. Notably, some characteristic biomolecules hold tremendous promise in guiding the synthesis of metal NCs with structure-related properties and subsequent biological applications. Continuous progress in multidisciplinary research has inspired the evolution of a variety of high-quality bio-inspired metal NCs to sustain a diverse library of functional building blocks, such as customizable size, core composition, molecular structure, and surface chemistry. These interesting properties, facilitate the assemblies and modularity of bio-inspired metal NCs with highly dimensional architectures, which could be combined with an array of other therapeutic systems for the spatiotemporal delivery and combination therapy delivery *in vitro* and *in vivo* models and early clinical trials[227–229].

Despite the considerable progress made in recent studies, some important challenges need to be addressed to maximize the therapeutic efficiency and accelerate the clinical application of bio-inspired metal NCs. Bio-inspired metal NCs as an emerging class of fluorescent materials usually exhibit size heterogeneity. Considering the close relevance of composition, structure, and properties, more attention should be paid to the accurate characterization of specific types, size, composition, and structure of metal NCs, as well as doped alloying, to impact the exploration of their precise therapeutic performance in specific applications. Furthermore, biomolecules stabilized metal NCs show a relatively low QY (often less than 10%) and fragile instability of metal clusters because of their tendency to undergo oxidation in response to an oxidative physiological condition or photoexcitation. Moreover, due to a lack of fundamental information and the mechanism of the bio-nano interface, a persistent challenge occurs in the assembly of ultrasmall particles into well-defined structures at the molecular level in an orderly manner. This is because the high surface energy of ultrasmall particles generally induces isotropic aggregation.

Biomolecules with desirable properties for metal NCs hold considerable promise for fabrication, multifunctionality, biosafety, and clinical translation. First, it has been demonstrated that characteristic biomolecules with rich chemical properties can be effectively utilized in the synthesis and assembly of metal NCs. The overall driven force from the characteristic sequence and spatial conformation of biomolecules, not only collectively achieve the controllable synthesis of atomically precise metal NCs, but also facilitate surface functionalization, large specific ratio surface area, molecular morphology, and highly ordered hierarchical structures in the sub-nanometer regime. Future studies should concentrate on the exploration of customized biomolecules and cells to promote the programmable synthesis of bio-inspired metal NCs with advanced biocomputation and machine learning. To avoid a sharp loss in the biological function and structural integrity of biomolecules, more attention should be paid to suitable synthesis conditions, such as mild synthesis condition, high quantum yielding, relatively pure production, and large-scale

preparation. Second, integrating inorganic metal NCs with biomolecules or cells could create multifunctional therapeutics and precisely spatiotemporal delivery, with properties such as variable surface functionalization, bio-responsiveness, and controllable payload release. On the one hand, biological studies have shown that biomolecules show extensive biological functions, responsiveness, and interactions in the physiological milieu, including molecular recognition, catalysis, and signal transduction. Such characteristic properties can be readily combined for the programmable design of bio-inspired metal NCs with combinatorial features and the instant response to external stimuli and signals. On the other hand, inorganic metal NCs provide unique optical, electronic, and catalytic properties, whereas biomolecules do not. Bio-inspired metal NCs should be explored for their size- and structure-dictated catalytic and therapeutic performance such as reduced off-site toxicity, enhanced therapeutic index, real-time monitoring, the enhanced immunologic effect of nanovaccines, radiotherapy, and phototherapy, as well as capability of nuclear targeting. Finally, compared with a large number of semiconductor and metal nanostructures, bio-inspired metal NCs show improved pharmacokinetic behavior profiles, including their good biological distribution, good biocompatibility, long-circulating ability, low immune response, and efficient renal clearance. In view of this, bio-inspired metal NCs can be artificially designed with stealth and low immune response as well as efficient renal clearance to avoid long-term accumulation in MPS organs (liver, spleen, etc.), which do not only reduce possible side effects but also facilitate successful clinical translation. As such, the combination of various biomolecules and specific metal NCs suggests great promise for the utilization of high-quality metal NCs as functional building blocks to construct novel supramolecular NPs or therapeutic systems.

We envision that this review provides a modular therapeutic platform integrating fluorescent imaging and therapeutic modalities, allowing for personalized medicine in the contexts of clinical translation. Our goal is to inspire researchers to understand the fabrication and design principles of bio-inspired metal NCs. This would facilitate the application of bio-inspired metal NCs in the integration with various cutting-edge modalities and techniques for multi-interdisciplinary engineering to address extensive biomedical issues, such as biosensing, bioimaging, biodistribution, biodefense, immune responsiveness, efficient delivery, and other diagnosis and combination therapy.

Acknowledgments

We express our cordial thanks for the support from Prof. Tiantian Kong. We are grateful to the support from National Natural Science Foundation of China (Grant No. 11802066) and Science and Technology Innovation Committee of Shenzhen (JCYJ20170818091601315, China). The authors are also thankful for the support from the China Postdoctoral Science Foundation (2019M01294501).

Author contributions

Dr. Peng Gao wrote the manuscript. Prof. Tianfu Wang revised the manuscript. All of the authors have edited and approved the final manuscript.

Conflicts of interest

There are no conflicts of interest to declare.

References

1. Wagner V, Dullaart A, Bock AK, Zweck A. The emerging nanomedicine landscape. *Nat Biotechnol* 2006;**24**:1211−7.
2. Sanhai WR, Sakamoto JH, Canady R, Ferrari M. Seven challenges for nanomedicine. *Nat Nanotechnol* 2008;**3**:242−4.
3. Bilia AR, Piazzini V, Guccione C, Risaliti L, Asprea M, Capecchi G, et al. Improving on nature: the role of nanomedicine in the development of clinical natural drugs. *Planta Med* 2017;**83**:366−81.
4. Kawasaki ES, Player A. Nanotechnology, nanomedicine, and the development of new, effective therapies for cancer. *Nanomedicine* 2005;**1**:101−9.
5. Katz E, Willner I. Integrated nanoparticle−biomolecule hybrid systems: synthesis, properties, and applications. *Angew Chem Int Ed* 2004;**43**:6042−108.
6. Chen Z, Wang Z, Gu Z. Bioinspired and biomimetic nanomedicines. *Acc Chem Res* 2019;**52**:1255−64.
7. Xie J, Zheng Y, Ying JY. Protein-directed synthesis of highly fluorescent gold nanoclusters. *J Am Chem Soc* 2009;**131**:888−9.
8. Conde J, Oliva N, Zhang Y, Artzi N. Local triple-combination therapy results in tumour regression and prevents recurrence in a colon cancer model. *Nat Mater* 2016;**15**:1128−38.
9. Ekkelenkamp AE, Elzes MR, Engbersen JF, Paulusse JM. Responsive crosslinked polymer nanogels for imaging and therapeutics delivery. *J Mater Chem B* 2018;**6**:210−35.
10. Song MF, Li YS, Kasai H, Kawai K. Metal nanoparticle-induced micronuclei and oxidative DNA damage in mice. *J Clin Biochem Nutr* 2011;**50**:211−6.
11. Sharma VK, Filip J, Zboril R, Varma RS. Natural inorganic nanoparticles−formation, fate, and toxicity in the environment. *Chem Soc Rev* 2015;**44**:8410−23.
12. Cassano D, Mapanao AK, Summa M, Vlamidis Y, Giannone G, Santi M, et al. Biosafety and biokinetics of noble metals: the impact of their chemical nature. *ACS Appl Bio Mater* 2019;**2**:4464−70.
13. Su Y, Xue T, Liu Y, Qi J, Jin R, Lin Z. Luminescent metal nanoclusters for biomedical applications. *Nano Res* 2019;**12**:1251−65.
14. Maity S, Bain D, Patra A. An overview on the current understanding of the photophysical properties of metal nanoclusters and their potential applications. *Nanoscale* 2019;**11**:22685−723.
15. Zheng K, Xie J. Engineering ultrasmall metal nanoclusters as promising theranostic agents. *Trends Chem* 2020;**2**:665−79.
16. Dickerson MB, Sandhage KH, Naik RR. Protein-and peptide-directed syntheses of inorganic materials. *Chem Rev* 2008;**108**:4935−78.
17. Yu Y, Luo Z, Teo CS, Tan YN, Xie J. Tailoring the protein conformation to synthesize different-sized gold nanoclusters. *Chem Commun* 2013;**49**:9740−2.
18. Cui R, Liu HH, Xie HY, Zhang ZL, Yang YR, Pang DW, et al. Living yeast cells as a controllable biosynthesizer for fluorescent quantum dots. *Adv Funct Mater* 2009;**19**:2359−64.
19. Richards CI, Choi S, Hsiang JC, Antoku Y, Vosch T, Bongiorno A, et al. Oligonucleotide-stabilized Ag sanocluster fluorophores. *J Am Chem Soc* 2008;**130**:5038−9.
20. Yuan X, Luo Z, Zhang Q, Zhang X, Zheng Y, Lee JY, et al. Synthesis of highly fluorescent metal (Ag, Au, Pt, and Cu) nanoclusters by electrostatically induced reversible phase transfer. *ACS Nano* 2011;**5**:8800−8.
21. Kairdolf BA, Smith AM, Stokes TH, Wang MD, Young AN, Nie S. Semiconductor quantum dots for bioimaging and biodiagnostic applications. *Annu Rev Anal Chem* 2013;**6**:143−62.
22. Wang H, Gao P, Wang Y, Guo J, Zhang KQ, Du D, et al. Fluorescently tuned nitrogen-doped carbon dots from carbon source with different content of carboxyl groups. *APL Mater* 2015;**3**:086102.

23. van de Linde S, Aufmkolk S, Franke C, Holm T, Klein T, Löschberger A, et al. Investigating cellular structures at the nanoscale with organic fluorophores. *Chem Biol* 2013;**20**:8−18.
24. Chen TW, Wardill TJ, Sun Y, Pulver SR, Renninger SL, Baohan A, et al. Ultrasensitive fluorescent proteins for imaging neuronal activity. *Nature* 2013;**499**:295−300.
25. Luo Z, Zheng K, Xie J. Engineering ultrasmall water-soluble gold and silver nanoclusters for biomedical applications. *Chem Commun* 2014;**50**:5143−55.
26. Cui ML, Zhao Y, Song Q. Synthesis, optical properties and applications of ultra-small luminescent gold nanoclusters. *Trac-Trend Anal Chem* 2014;**57**:73−82.
27. Srinivasulu YG, Yao Q, Goswami N, Xie J. Interfacial engineering of gold nanoclusters for biomedical applications. *Mater Horiz* 2020;**7**: 2596−618.
28. Liu J, Yu M, Zhou C, Zheng J. Renal clearable inorganic nanoparticles: a new frontier of bionanotechnology. *Mater Today* 2013;**16**: 477−86.
29. Yu M, Zhou J, Du B, Ning X, Authement C, Gandee L, et al. Noninvasive Staging of kidney dysfunction enabled by renal-clearable luminescent gold nanoparticles. *Angew Chem Int Ed* 2016;**55**:2787−91.
30. Du B, Jiang X, Das A, Zhou Q, Yu M, Jin R, et al. Glomerular barrier behaves as an atomically precise bandpass filter in a sub-nanometre regime. *Nat Nanotechnol* 2017;**12**:1096.
31. Tao Y, Li M, Ren J, Qu X. Metal nanoclusters: novel probes for diagnostic and therapeutic applications. *Chem Soc Rev* 2015;**44**: 8636−63.
32. Song XR, Goswami N, Yang HH, Xie J. Functionalization of metal nanoclusters for biomedical applications. *Analyst* 2016;**141**: 3126−40.
33. Wang B, Zhao M, Mehdi M, Wang G, Gao P, Zhang KQ. Biomolecule-assisted synthesis and functionality of metal nanoclusters for biological sensing: a review. *Mater Chem Front* 2019;**3**:1722−35.
34. Fosgerau K, Hoffmann T. Peptide therapeutics: current status and future directions. *Drug Discov Today* 2015;**20**:122−8.
35. Frokjaer S, Otzen DE. Protein drug stability: a formulation challenge. *Nat Rev Drug Discov* 2005;**4**:298−306.
36. Higaki T, Li Y, Zhao S, Li Q, Li S, Du XS, et al. Atomically tailored gold nanoclusters for catalytic application. *Angew Chem Int Ed* 2019; **131**:8377−88.
37. Wu Z, Yao Q, Zang S, Xie J. Directed self-assembly of ultrasmall metal nanoclusters. *ACS Mater Lett* 2019;**1**:237−48.
38. Yao Q, Chen T, Yuan X, Xie J. Toward total synthesis of thiolate-protected metal nanoclusters. *Acc Chem Res* 2018;**51**:1338−48.
39. Zhou T, Huang Y, Li W, Cai Z, Luo F, Yang CJ, et al. Facile synthesis of red-emitting lysozyme-stabilized Ag nanoclusters. *Nanoscale* 2012;**4**:5312−5.
40. Ghosh R, Sahoo AK, Ghosh SS, Paul A, Chattopadhyay A. Blue-emitting copper nanoclusters synthesized in the presence of lysozyme as candidates for cell Labeling. *ACS Appl Mater Interfaces* 2014;**6**:3822−8.
41. Yu CJ, Chen TH, Jiang JY, Tseng WL. Lysozyme-directed synthesis of platinum nanoclusters as a mimic oxidase. *Nanoscale* 2014;**6**: 9618−24.
42. Lin YH, Tseng WL. Ultrasensitive sensing of Hg^{2+} and CH_3Hg^+ based on the fluorescence quenching of lysozyme type VI-stabilized gold nanoclusters. *Anal Chem* 2010;**82**:9194−200.
43. Sun C, Yang H, Yuan Y, Tian X, Wang L, Guo Y, et al. Controlling assembly of paired gold clusters within apoferritin nanoreactor for *in vivo* kidney targeting and biomedical imaging. *J Am Chem Soc* 2011;**133**:8617−24.
44. Kawasaki H, Hamaguchi K, Osaka I, Arakawa R. PH-dependent synthesis of pepsin-mediated gold nanoclusters with blue green and red fluorescent emission. *Adv Funct Mater* 2011;**21**:3508−15.
45. Kong Y, Chen J, Gao F, Brydson R, Johnson B, Heath G, et al. Near-infrared fluorescent ribonuclease-A-encapsulated gold nanoclusters: preparation, characterization, cancer targeting and imaging. *Nanoscale* 2013;**5**:1009−17.
46. Wang Y, Cui Y, Zhao Y, Liu R, Sun Z, Li W, et al. Bifunctional peptides that precisely biomineralize Au clusters and specifically stain cell nuclei. *Chem Commun* 2012;**48**:871−3.
47. Yu JH, Patel SA, Dickson RM. *In vitro* and intracellular production of peptide-encapsulated fluorescent silver nanoclusters. *Angew Chem Int Ed* 2007;**46**:2028−30.
48. Lan GY, Chen WY, Chang HT. One-pot synthesis of fluorescent oligonucleotide Ag nanoclusters for specific and sensitive detection of DNA. *Biosens Bioelectron* 2011;**26**:2431−5.
49. Yu Y, Luo Z, Yu Y, Lee JY, Xie J. Observation of cluster size growth in CO-directed synthesis of $Au_{25}(SR)_{18}$ nanoclusters. *ACS Nano* 2012;**6**:7920−7.
50. Aires A, Llarena I, Moller M, Castro-Smirnov J, Cabanillas-Gonzalez J, Cortajarena AL. A simple approach to design proteins for the sustainable synthesis of metal nanoclusters. *Angew Chem Int Ed* 2019;**58**:6214−9.
51. Chen D, Zhao C, Ye J, Li Q, Liu X, Su M, et al. *In situ* biosynthesis of fluorescent platinum nanoclusters: toward self-bioimaging-guided cancer theranostics. *ACS Appl Mater Interfaces* 2015;**7**:18163−9.
52. Muhammed MAH, Verma PK, Pal SK, Retnakumari A, Koyakutty M, Nair S, et al. Luminescent quantum clusters of gold in bulk by albumin-induced core etching of nanoparticles: metal ion sensing, metal-enhanced luminescence, and biolabeling. *Chem Eur J* 2010;**16**:10103−12.
53. Zhou R, Shi M, Chen X, Wang M, Chen H. Atomically monodispersed and fluorescent sub-nanometer gold clusters created by biomolecule-assisted etching of nanometer-sized gold particles and rods. *Chem Eur J* 2009;**15**:4944−51.
54. Le Guével X, Trouillet V, Spies C, Jung G, Schneider M. Synthesis of yellow-emitting platinum nanoclusters by ligand etching. *J Phys Chem C* 2012;**116**:6047−51.
55. Yuan X, Zhang B, Luo Z, Yao Q, Leong DT, Yan N, et al. Balancing the rate of cluster growth and etching for gram-scale synthesis of thiolate-protected Au_{25} nanoclusters with atomic precision. *Angew Chem Int Ed* 2014;**53**:4623−7.
56. Wang Y, Chen J, Irudayaraj J. Nuclear Targeting dynamics of gold nanoclusters for enhanced therapy of HER^{2+} breast cancer. *ACS Nano* 2011;**5**:9718−25.
57. Khlebtsov BN, Tuchina ES, Tuchin VV, Khlebtsov N. Multifunctional Au nanoclusters for targeted bioimaging and enhanced photodynamic inactivation of Staphylococcus aureus. *RSC Adv* 2015; **5**:61639−49.
58. Yu J, Choi S, Richards CI, Antoku Y, Dickson RM. Live cell surface labeling with fluorescent Ag nanocluster conjugates. *Photochem Photobiol* 2008;**84**:1435−9.
59. Zhang S. Fabrication of novel biomaterials through molecular self-assembly. *Nat Biotechnol* 2003;**21**:1171−8.
60. Grzelczak M, Vermant J, Furst EM, Liz-Marzán LM. Directed self-assembly of nanoparticles. *ACS Nano* 2010;**4**:3591−605.
61. Li Z, Peng H, Liu J, Tian Y, Yang W, Yao J, et al. Plant protein-directed synthesis of luminescent gold nanocluster hybrids for tumor imaging. *ACS Appl Mater Interfaces* 2018;**10**:83−90.
62. Zhang W, Lin D, Wang H, Li J, Nienhaus GU, Su Z, et al. Supramolecular self-assembly bioinspired synthesis of luminescent gold nanocluster-embedded peptide nanofibers for temperature sensing and cellular imaging. *Bioconjugate Chem* 2017;**28**:2224−9.
63. Nair LV, Philips DS, Jayasree RS, Ajayaghosh A. A Near-infrared fluorescent nanosensor (AuC@Urease) for the selective detection of blood urea. *Small* 2013;**9**:2673−7.
64. Lyu DY, Li J, Wang XW, Guo WW, Wang EK. Cationic-polyelectrolyte-modified fluorescent DNA−silver nanoclusters with enhanced emission and higher stability for rapid bioimaging. *Anal Chem* 2019;**91**:2050−7.
65. Díez I, Ras RHA. Fluorescent silver nanoclusters. *Nanoscale* 2011;**3**: 1963−70.

66. Qian H, Zhu M, Wu Z, Jin R. Quantum sized gold nanoclusters with atomic precision. *Acc Chem Res* 2012;**45**:1470−9.
67. Tracy JB, Kalyuzhny G, Crowe MC, Balasubramanian R, Choi JP, Murray RW. Poly(ethylene glycol) ligands for high-resolution nanoparticle mass spectrometry. *J Am Chem Soc* 2007;**129**:6706−7.
68. Yu Y, Luo Z, Chevrier DM, Leong DT, Zhang P, Jiang DE, et al. Identification of a highly luminescent $Au_{22}(SG)_{18}$ nanocluster. *J Am Chem Soc* 2014;**136**:1246−9.
69. Yuan X, Setyawati MI, Tan AS, Ong CN, Leong DT, Xie J. Highly luminescent silver nanoclusters with tunable emissions: cyclic reduction−decomposition synthesis and antimicrobial properties. *NPG Asia Mater* 2013;**5**:e39.
70. Bootharaju MS, Joshi CP, Parida MR, Mohammed OF, Bakr OM. Templated atom-precise galvanic synthesis and structure elucidation of a $[Ag_{24}Au(SR)_{18}]^-$ nanocluster. *Angew Chem Int Ed* 2016;**55**:922−6.
71. Zhang N, Si Y, Sun Z, Chen L, Li R, Qiao Y, et al. Rapid, Selective, and ultrasensitive fluorimetric analysis of mercury and copper levels in blood using bimetallic gold−silver nanoclusters with "silver effect"-enhanced red fluorescence. *Anal Chem* 2014;**86**:11714−21.
72. Wu Z, Jin R. On the ligand's role in the fluorescence of gold nanoclusters. *Nano Lett* 2010;**10**:2568−73.
73. Chang HY, Chang HT, Hung YL, Hsiung TM, Lin YW, Huang CC. Ligand effect on the luminescence of gold nanodots and its application for detection of total mercury ions in biological samples. *RSC Adv* 2013;**3**:4588−97.
74. Zhu M, Aikens CM, Hollander FJ, Schatz GC, Jin R. Correlating the crystal structure of A thiol-protected Au_{25} cluster and optical properties. *J Am Chem Soc* 2008;**130**:5883−5.
75. Qian H, Eckenhoff WT, Zhu Y, Pintauer T, Jin R. Total Structure determination of thiolate-protected Au_{38} nanoparticles. *J Am Chem Soc* 2010;**132**:8280−1.
76. Negishi Y, Nobusada K, Tsukuda T. Glutathione-protected gold clusters revisited: bridging the gap between gold(I)−thiolate complexes and thiolate-protected gold nanocrystals. *J Am Chem Soc* 2005;**127**:5261−70.
77. Petty JT, Zheng J, Hud NV, Dickson RM. DNA-templated Ag nanocluster formation. *J Am Chem Soc* 2004;**126**:5207−12.
78. Adhikari B, Banerjee A. Facile synthesis of water-soluble fluorescent silver nanoclusters and hg (II) sensing. *Chem Mater* 2010;**22**:4364−71.
79. Baksi A, Bootharaju MS, Chen X, Häkkinen H, Pradeep T. $Ag_{11}(SG)_7$: a new cluster identified by mass spectrometry and optical spectroscopy. *J Phys Chem C* 2014;**118**:21722−9.
80. Bhamore JR, Deshmukh B, Haran V, Jha S, Singhal RK, Lenka N, et al. One-step eco-friendly approach for the fabrication of synergistically engineered fluorescent copper nanoclusters: sensing of Hg^{2+} ion and cellular uptake and bioimaging properties. *New J Chem* 2018;**42**:1510−20.
81. Xu N, Li HW, Wu Y. Hydrothermal synthesis of polyethylenimine-protected high luminescent Pt-nanoclusters and their application to the detection of nitroimidazoles. *Anal Chim Acta* 2017;**958**:51−8.
82. Huang T, Murray RW. Luminescence of tiopronin monolayer-protected silver clusters changes to that of gold clusters upon galvanic core metal exchange. *J Phys Chem B* 2003;**107**:7434−40.
83. Link S, Beeby A, FitzGerald S, El-Sayed MA, Schaaff TG, Whetten RL. Visible to infrared luminescence from a 28-atom gold cluster. *J Phys Chem B* 2002;**106**:3410−5.
84. Huang CC, H YL, Shiang YC, Lin TY, Lin YS, Chen CT, et al. Photoassisted synthesis of luminescent mannose-Au nanodots for the detection of thyroglobulin in serum. *Chem Asian J* 2010;**5**:334−41.
85. Huang T, Murray RW. Visible luminescence of water-soluble monolayer-protected gold clusters. *J Phys Chem B* 2001;**105**:12498−502.
86. Squirrell JM, Wokosin DL, White JG, Bavister BD. Long-term two-photon fluorescence imaging of mammalian embryos without compromising viability. *Nat Biotechnol* 1999;**17**:763.
87. Ramakrishna G, Varnavski O, Kim J, Lee D, Goodson T. Quantum-sized gold clusters as efficient two-photon absorbers. *J Am Chem Soc* 2008;**130**:5032−3.
88. Polavarapu L, Manna M, Xu QH. Biocompatible glutathione capped gold clusters as one- and two-photon excitation fluorescence contrast agents for live cells imaging. *Nanoscale* 2011;**3**:429−34.
89. Patel SA, Richards CI, Hsiang JC, Dickson RM. Water-soluble Ag nanoclusters exhibit strong two-photon-induced fluorescence. *J Am Chem Soc* 2008;**130**:11602−3.
90. Isabelle RA, Bertorelle F, Hamouda R, Rayane D, Dugourd P, Sanader Ž, et al. Tuning Ag29 nanocluster light emission from red to blue with one and two-photon excitation. *Nanoscale* 2016;**8**:2892−8.
91. Wang Y, Cui Y, Liu R, Wei Y, Jiang X, Zhu H, et al. Blue two-photon fluorescence metal cluster probe precisely marking cell nuclei of two cell lines. *Chem Commun* 2013;**49**:10724−6.
92. Zhang H, Zhao Z, McGonigal PR, Ye R, Liu S, Lam JWY, et al. Clusterization-triggered emission: uncommon luminescence from common materials. *Mater Today* 2020;**32**:275−92.
93. Jin Y, Li S, Han Z, Yan BJ, Zang SQ. Cations controlling the chiral assembly of luminescent atomically precise copper(I) clusters. *Angew Chem Int Ed* 2019;**131**:12271−6.
94. Wu Z, Yao Q, Chai OJH, Ding N, Xu W, Zang S, et al. Unraveling the impact of gold(I)−thiolate motifs on the aggregation induced emission of gold nanoclusters. *Angew Chem Int Ed* 2020;**59**:9934−9.
95. Wu Z, Du Y, Liu J, Yao Q, Chen T, Cao Y, et al. Aurophilic interactions in the self-assembly of gold nanoclusters into nanoribbons with enhanced luminescence. *Angew Chem Int Ed* 2019;**58**:8139−44.
96. Luo Z, Yuan X, Yu Y, Zhang Q, Leong DT, Lee JY, et al. From aggregation-induced emission of Au(I)−thiolate complexes to ultrabright Au(0)@Au(I)−thiolate core−shell nanoclusters. *J Am Chem Soc* 2012;**134**:16662−70.
97. Zheng K, Yuan X, Kuah K, Luo Z, Yao Q, Zhang Q, et al. Boiling water synthesis of ultrastable thiolated silver nanoclusters with aggregation-induced emission. *Chem Commun* 2015;**51**:15165−8.
98. Jia X, Yang X, Li J, Li D, Wang E. Stable Cu nanoclusters: from an aggregation-induced emission mechanism to biosensing and catalytic applications. *Chem Commun* 2014;**50**:237−9.
99. Zhang G, Wang R, Shi L, Zhang C, Zhang Y, Zhou Y, et al. Aggregation/assembly induced emission based on silk fibroin-templated fluorescent copper nanoclusters for "turn-on" detection of S^{2-}. *Sensor Actuator B Chem* 2019;**279**:361−8.
100. Wang Z, Zhu Z, Zhao C, Yao Q, Li X, Liu H, et al. Silver doping-induced luminescence enhancement and red-shift of gold nanoclusters with aggregation-induced emission. *Chem Asian J* 2019;**14**:765−9.
101. Jalili R, Khataee A. Aluminum(III) triggered aggregation-induced emission of glutathione-capped copper nanoclusters as a fluorescent probe for creatinine. *Microchim Acta* 2018;**186**:29.
102. Narayanan SS, Pal SK. Structural and functional characterization of luminescent silver−protein nanobioconjugates. *J Phys Chem C* 2008;**112**:4874−9.
103. Zhao T, He XW, Li WY, Zhang Y. Transferrin-directed preparation of red-emitting copper nanoclusters for targeted imaging of transferrin receptor over-expressed cancer cells. *J Mater Chem B* 2015;**3**:2388−94.
104. Zhang S, Zhang X, Su Z. Biomolecule conjugated metal nanoclusters: bio-inspiration strategies, targeted therapeutics, and diagnostics. *J Mater Chem B* 2020;**8**:4176−94.
105. Liu R, Wang Y, Yuan Q, An D, Li J, Gao X. The Au clusters induce tumor cell apoptosis *via* specifically targeting thioredoxin reductase 1 (TrxR1) and suppressing its activity. *Chem Commun* 2014;**50**:10687−90.
106. Liu J. DNA-stabilized, fluorescent, metal nanoclusters for biosensor development. *Trac-Trends Anal Chem* 2014;**58**:99−111.
107. Zhang S, Wang K, Li KB, Shi W, Jia WP, Chen X, et al. A DNA-stabilized silver nanoclusters/graphene oxide-based platform for the sensitive detection of DNA through hybridization chain reaction. *Biosens Bioelectron* 2017;**91**:374−9.

108. Zhou Y, Wang H, Zhang H, Chai YQ, Yuan R. Programmable modulation of copper nanoclusters electrochemiluminescence *via* DNA nanocranes for ultrasensitive detection of microRNA. *Anal Chem* 2018;**90**:3543−9.
109. Huang Y, He S, Cao W, Cai K, Liang XJ. Biomedical nanomaterials for imaging-guided cancer therapy. *Nanoscale* 2012;**4**:6135−49.
110. Yuan Q, Wang Y, Zhao L, Liu R, Gao F, Gao L, et al. Peptide protected gold clusters: chemical synthesis and biomedical applications. *Nanoscale* 2016;**8**:12095−104.
111. Zhang L, Wang E. Metal nanoclusters: new fluorescent probes for sensors and bioimaging. *Nano Today* 2014;**9**:132−57.
112. Palmal S, Jana NR. Gold nanoclusters with enhanced tunable fluorescence as bioimaging probes. *Wires Nanomed Nanobi* 2014;**6**: 102−10.
113. Liu H, Hong G, Luo Z, Chen J, Chang J, Gong M, et al. Atomic-precision gold clusters for NIR-II imaging. *Adv Mater* 2019;**31**: 1901015.
114. Yu J, Patel SA, Dickson RM. *In vitro* and intracellular production of peptide-encapsulated fluorescent silver nanoclusters. *Angew Chem Int Ed* 2007;**119**:2074−6.
115. Gao P, Wang H, Zou G, Zhang KQ. Silk fibroin-derived peptide directed silver nanoclusters for cell imaging. *RSC Adv* 2018;**8**: 27805−10.
116. Huang H, Li H, Wang AJ, Zhong SX, Fang KM, Feng JJ. Green synthesis of peptide-templated fluorescent copper nanoclusters for temperature sensing and cellular imaging. *Analyst* 2014;**139**: 6536−41.
117. Le Guével X, Spies C, Daum N, Jung G, Schneider M. Highly fluorescent silver nanoclusters stabilized by glutathione: a promising fluorescent label for bioimaging. *Nano Res* 2012;**5**:379−87.
118. Das NK, Ghosh S, Priya A, Datta S, Mukherjee S. Luminescent copper nanoclusters as a specific cell-imaging probe and a selective metal ion sensor. *J Phys Chem C* 2015;**119**:24657−64.
119. Liu CL, Wu HT, Hsiao YH, Lai CW, Shih CW, Peng YK, et al. Insulin-directed synthesis of fluorescent gold nanoclusters: preservation of insulin bioactivity and versatility in cell imaging. *Angew Chem Int Ed* 2011;**50**:7056−60.
120. Gao P, Wu S, Chang X, Liu F, Zhang T, Wang B, et al. Aprotinin encapsulated gold nanoclusters: a fluorescent bioprobe with dynamic nuclear targeting and selective detection of trypsin and heavy metal. *Bioconjugate Chem* 2018;**29**:4140−8.
121. Le Guével X, Daum N, Schneider M. Synthesis and characterization of human transferrin-stabilized gold nanoclusters. *Nanotechnology* 2011;**22**:275103.
122. Retnakumari A, Setua S, Menon D, Ravindran P, Muhammed H, Pradeep T, et al. Molecular-receptor-specific, non-toxic, near-infrared-emitting Au cluster-protein nanoconjugates for targeted cancer imaging. *Nanotechnology* 2009;**21**:055103.
123. Habeeb Muhammed MA, Verma PK, Pal SK, Retnakumari A, Koyakutty M, Nair S, et al. Luminescent quantum clusters of gold in bulk by albumin-induced core etching of nanoparticles: metal ion sensing, metal-enhanced luminescence, and biolabeling. *Chem Eur J* 2010;**16**:10103−12.
124. Qiao J, Mu X, Qi L, Deng J, Mao L. Folic acid-functionalized fluorescent gold nanoclusters with polymers as linkers for cancer cell imaging. *Chem Commun* 2013;**49**:8030−2.
125. Choi S, Dickson RM, Yu J. Developing luminescent silver nanodots for biological applications. *Chem Soc Rev* 2012;**41**:1867−91.
126. Choi S, Yu JH, Patel SA, Tzeng YL, Dickson RM. Tailoring silver nanodots for intracellular staining. *Photochem Photobiol Sci* 2011; **10**:109−15.
127. Sun Z, Wang Y, Wei Y, Liu R, Zhu H, Cui Y, et al. Ag cluster−aptamer hybrid: specifically marking the nucleus of live cells. *Chem Commun* 2011;**47**:11960−2.
128. Ghoroghchian PP, Therien MJ, Hammer DA. *In vivo* fluorescence imaging: a personal perspective. *Wires Nanomed Nanobi* 2009;**1**: 156−67.
129. Shang L, Nienhaus GU. Gold nanoclusters as novel optical probes for *in vitro* and *in vivo* fluorescence imaging. *Biophys Rev* 2012;**4**: 313−22.
130. Zhou C, Long M, Qin Y, Sun X, Zheng J. Luminescent gold nanoparticles with efficient renal clearance. *Angew Chem Int Ed* 2011;**50**: 3168−72.
131. Liu J, Yu M, Zhou C, Yang S, Ning X, Zheng J. Passive tumor targeting of renal-clearable luminescent gold nanoparticles: long tumor retention and fast normal tissue clearance. *J Am Chem Soc* 2013;**135**: 4978−81.
132. Zhang C, Zhou Z, Qian Q, Gao G, Li C, Feng L, et al. Glutathione-capped fluorescent gold nanoclusters for dual-modal fluorescence/X-ray computed tomography imaging. *J Mater Chem B* 2013;**1**: 5045−53.
133. Wu X, He X, Wang K, Xie C, Zhou B, Qing Z. Ultrasmall near-infrared gold nanoclusters for tumor fluorescence imaging *in vivo*. *Nanoscale* 2010;**2**:2244−9.
134. Liu X, Wang F, Aizen R, Yehezkeli O, Willner I. Graphene oxide/nucleic-acid-stabilized silver nanoclusters: functional hybrid materials for optical aptamer sensing and multiplexed analysis of pathogenic DNAs. *J Am Chem Soc* 2013;**135**:11832−9.
135. Thakkar KN, Mhatre SS, Parikh RY. Biological synthesis of metallic nanoparticles. *Nanomedicine* 2010;**6**:257−62.
136. Huang J, Lin L, Sun D, Chen H, Yang D, Li Q. Bio-inspired synthesis of metal nanomaterials and applications. *Chem Soc Rev* 2015;**44**: 6330−74.
137. Wang J, Zhang G, Li Q, Jiang H, Liu C, Amatore C, et al. *In vivo* self-bio-imaging of tumors through in situ biosynthesized fluorescent gold nanoclusters. *Sci Rep* 2013;**3**:1157.
138. Gao S, Chen D, Li Q, Ye J, Jiang H, Amatore C, et al. Near-infrared fluorescence imaging of cancer cells and tumors through specific biosynthesis of silver nanoclusters. *Sci Rep* 2014;**4**:4384.
139. Hu H, Huang P, Weiss OJ, Yan X, Yue X, Zhang MG, et al. PET and NIR optical imaging using self-illuminating 64 Cu-doped chelator-free gold nanoclusters. *Biomaterials* 2014;**35**:9868−76.
140. Goswami N, Luo Z, Yuan X, Leong DT, Xie J. Engineering gold-based radiosensitizers for cancer radiotherapy. *Mater Horiz* 2017;**4**: 817−31.
141. Pan Y, Leifert A, Ruau D, Neuss S, Bornemann J, Schmid G, et al. Gold Nanoparticles of diameter 1.4 nm trigger necrosis by oxidative stress and mitochondrial damage. *Small* 2009;**5**:2067−76.
142. Ghahremani F, Shahbazi-Gahrouei D, Kefayat A, Motaghi H, Mehrgardi MA, Javanmard SH. AS1411 aptamer conjugated gold nanoclusters as a targeted radiosensitizer for megavoltage radiation therapy of 4T1 breast cancer cells. *RSC Adv* 2018;**8**: 4249−58.
143. Zhang XD, Luo Z, Chen J, Shen X, Song S, Sun Y, et al. Ultrasmall Au_{10-12} $(SG)_{10-12}$ nanomolecules for high tumor specificity and cancer radiotherapy. *Adv Mater* 2014;**26**:4565−8.
144. Zhang XD, Luo Z, Chen J, Song S, Yuan X, Shen X, et al. Ultrasmall glutathione-protected gold nanoclusters as next generation radiotherapy sensitizers with high tumor uptake and high renal clearance. *Sci Rep* 2015;**5**:8669.
145. Zhang XD, Chen J, Luo Z, Wu D, Shen X, Song SS, et al. Enhanced tumor accumulation of Sub-2 nm gold nanoclusters for cancer radiation therapy. *Adv healthc mater* 2014;**3**:133−41.
146. Liang G, Jin X, Zhang S, Xing D. RGD peptide-modified fluorescent gold nanoclusters as highly efficient tumor-targeted radiotherapy sensitizers. *Biomaterials* 2017;**144**:95−104.
147. Fang X, Wang Y, Ma X, Li Y, Zhang Z, Xiao Z, et al. Mitochondria-targeting Au nanoclusters enhance radiosensitivity of cancer cells. *J Mater Chem B* 2017;**5**:4190−7.
148. Shibu ES, Hamada M, Murase N, Biju V. Nanomaterials formulations for photothermal and photodynamic therapy of cancer. *J Photoch Photobio C* 2013;**15**:53−72.
149. Liu J, Detrembleur C, Pauw-Gillet MCD, Mornet S, Jérôme C, Duguet E. Gold nanorods coated with mesoporous silica shell as drug

delivery system for remote near infrared light-activated release and potential phototherapy. *Small* 2015;**11**:2323−32.
150. Celli JP, Spring BQ, Rizvi I, Evans CL, Samkoe KS, Verma S, et al. Imaging and photodynamic therapy: mechanisms, monitoring, and optimization. *Chem Rev* 2010;**110**:2795−838.
151. Zhang C, Li C, Liu Y, Zhang J, Bao C, Liang S, et al. Gold nanoclusters-based nanoprobes for simultaneous fluorescence imaging and targeted photodynamic therapy with superior penetration and retention behavior in tumors. *Adv Funct Mater* 2015;**25**:1314−25.
152. Huang P, Lin J, Wang S, Zhou Z, Li Z, Wang Z, et al. Photosensitizer-conjugated silica-coated gold nanoclusters for fluorescence imaging-guided photodynamic therapy. *Biomaterials* 2013;**34**:4643−54.
153. Li Y, Jian X, Zhou S, Lu Y, Zhao C, Gao Z, et al. Protein shell-encapsulated Pt clusters as continuous O_2-supplied biocoats for photodynamic therapy in hypoxic cancer cells. *ACS Appl Mater Interfaces* 2019;**11**:17215−25.
154. Kawasaki H, Kumar S, Li G, Zeng C, Kauffman DR, Yoshimoto J, et al. Generation of singlet oxygen by photoexcited Au25(SR)18 clusters. *Chem Mater* 2014;**26**:2777−88.
155. Agrachev M, Fei W, Antonello S, Bonacchi S, Dainese T, Zoleo A, et al. Understanding and controlling the efficiency of $Au_{24}M(SR)_{18}$ nanoclusters as singlet-oxygen photosensitizers. *Chem Sci* 2020;**11**:3427−40.
156. Vankayala R, Kuo CL, Nuthalapati K, Chiang CS, Hwang KC. Nucleus-targeting gold nanoclusters for simultaneous *in vivo* fluorescence imaging, gene delivery, and NIR-light activated photodynamic therapy. *Adv Funct Mater* 2015;**25**:5934−45.
157. Chen D, Gao S, Ge W, Li Q, Jiang H, Wang X. One-step rapid synthesis of fluorescent platinum nanoclusters for cellular imaging and photothermal treatment. *RSC Adv* 2014;**4**:40141−5.
158. Gu W, Zhang Q, Zhang T, Li Y, Xiang J, Peng R, et al. Hybrid polymeric nano-capsules loaded with gold nanoclusters and indocyanine green for dual-modal imaging and photothermal therapy. *J Mater Chem B* 2016;**4**:910−9.
159. Otvos L, Wade JD. Current challenges in peptide-based drug discovery. *Front Chem* 2014;**2**:62.
160. Kim YT, Kim KH, Kang ES, Jo G, Ahn SY, Park SH, et al. Synergistic effect of detection and separation for pathogen using magnetic clusters. *Bioconjug Chem* 2016;**27**:59−65.
161. Söderberg A, Sahaf B, Rosén A. Thioredoxin reductase, a redox-active selenoprotein, is secreted by normal and neoplastic cells: presence in human plasma. *Cancer Res* 2000;**60**:2281−9.
162. Li Q, Yuan Q, Zhao M, Yao Y, Gao L, Liu R, et al. Au nanoclusters suppress chronic lymphocytic leukaemia cells by inhibiting thioredoxin reductase 1 to induce intracellular oxidative stress and apoptosis. *Sci Bull* 2017;**62**:537−45.
163. Zhao JY, Cui R, Zhang ZL, Zhang M, Xie ZX, Pang DW. Cytotoxicity of nucleus-targeting fluorescent gold nanoclusters. *Nanoscale* 2014;**6**:13126−34.
164. An D, Su J, Weber JK, Gao X, Zhou R, Li J. A Peptide-coated gold nanocluster exhibits unique behavior in protein activity inhibition. *J Am Chem Soc* 2015;**137**:8412−8.
165. Liu M, Gao L, Zhao L, He J, Yuan Q, Zhang P, et al. Peptide-Au clusters induced tumor cells apoptosis *via* targeting glutathione peroxidase-1: the molecular dynamics assisted experimental studies. *Sci Rep* 2017;**7**:131.
166. Xia H, Li F, Hu X, Park W, Wang S, Jang Y, et al. pH-Sensitive Pt nanocluster assembly overcomes cisplatin resistance and heterogeneous stemness of hepatocellular carcinoma. *ACS Cent Sci* 2016;**2**:802−11.
167. Zhai J, Jia Y, Zhao L, Yuan Q, Gao F, Zhang X, et al. Turning on/off the anti-tumor effect of the Au cluster *via* atomically controlling its molecular size. *ACS Nano* 2018;**12**:4378−86.
168. Chen H, Li S, Li B, Ren X, Li S, Mahounga DM, et al. Folate-modified gold nanoclusters as near-infrared fluorescent probes for tumor imaging and therapy. *Nanoscale* 2012;**4**:6050−64.
169. Zhou F, Feng B, Yu H, Wang D, Wang T, Liu J, et al. Cisplatin prodrug-conjugated gold nanocluster for fluorescence imaging and targeted therapy of the breast cancer. *Theranostics* 2016;**6**:679−87.
170. Chen H, Li B, Ren X, Li S, Ma Y, Cui S, et al. Multifunctional near-infrared-emitting nano-conjugates based on gold clusters for tumor imaging and therapy. *Biomaterials* 2012;**33**:8461−76.
171. Plotkin SA, Plotkin SL. The development of vaccines: how the past led to the future. *Nat Rev Microbiol* 2011;**9**:889−93.
172. Plotkin S. History of vaccination. *Proc Natl Acad Sci U S A* 2014;**111**:12283−7.
173. Hubbell JA, Thomas SN, Swartz MA. Materials engineering for immunomodulation. *Nature* 2009;**462**:449−60.
174. Liu Y, Chen C. Role of nanotechnology in HIV/AIDS vaccine development. *Adv Drug Deliv Rev* 2016;**103**:76−89.
175. Kroll AV, Jiang Y, Zhou J, Holay M, Fang RH, Zhang L. Biomimetic nanoparticle vaccines for cancer therapy. *Adv biosystems* 2019;**3**:1800219.
176. Vollmer J, Krieg AM. Immunotherapeutic applications of CpG oligodeoxynucleotide TLR9 agonists. *Adv Drug Deliv Rev* 2009;**61**:195−204.
177. Takahashi Y, Serada S, Hiramatsu K, Kobiyama K, Fujimoto M, Ishii K, et al. The antitumor efficacy of anti-BST2 antibody is significantly increased in combination with CpG oligodeoxynucleotide in endometrial cancer. *Cancer Res* 2015;**75**:2487.
178. Tao Y, Li Z, Ju E, Ren J, Qu X. One-step DNA-programmed growth of CpG conjugated silver nanoclusters: a potential platform for simultaneous enhanced immune response and cell imaging. *Chem Commun* 2013;**49**:6918−20.
179. Tao Y, Ju E, Li Z, Ren J, Qu X. Engineered CpG-antigen conjugates protected gold nanoclusters as smart self-vaccines for enhanced immune response and cell imaging. *Adv Funct Mater* 2014;**24**:1004−10.
180. Tao Y, Zhang Y, Ju E, Ren H, Ren J. Gold nanocluster-based vaccines for dual-delivery of antigens and immunostimulatory oligonucleotides. *Nanoscale* 2015;**7**:12419−26.
181. Peer D, Karp JM, Hong S, Farokhzad OC, Margalit R, Langer R. Nanocarriers as an emerging platform for cancer therapy. *Nat Nanotechnol* 2007;**2**:751−60.
182. He Y, Zhang W, Guo T, Zhang G, Qin W, Zhang L, et al. Drug nanoclusters formed in confined nano-cages of CD-MOF: dramatic enhancement of solubility and bioavailability of azilsartan. *Acta Pharm Sin B* 2019;**9**:97−106.
183. Dachs GU, Dougherty GJ, Stratford IJ, Chaplin DJ. Targeting gene therapy to cancer: a review. *Oncol Res* 1997;**9**:313−25.
184. El-Aneed A. An overview of current delivery systems in cancer gene therapy. *J Control Release* 2004;**94**:1−14.
185. Naldini L. Gene therapy returns to centre stage. *Nature* 2015;**526**:351−60.
186. Li J, Wang W, Sun D, Chen J, Zhang PH, Zhang JR, et al. Aptamer-functionalized silver nanoclusters-mediated cell type-specific siRNA delivery and tracking. *Chem Sci* 2013;**4**:3514−21.
187. Dutta D, Chattopadhyay A, Ghosh SS. Cationic BSA templated Au−Ag bimetallic nanoclusters as a theranostic gene delivery vector for HeLa cancer cells. *ACS Biomater Sci Eng* 2016;**2**:2090−8.
188. Sarparast M, Noori A, Ilkhani H, Bathaie SZ, El-Kady MF, Wang LJ, et al. Cadmium nanoclusters in a protein matrix: synthesis, characterization, and application in targeted drug delivery and cellular imaging. *Nano Res* 2016;**9**:3229−46.
189. Lei Y, Tang L, Xie Y, Xianyu Y, Zhang L, Wang P, et al. Gold nanoclusters-assisted delivery of NGF siRNA for effective treatment of pancreatic cancer. *Nat Commun* 2017;**8**:15130.
190. Spellberg B, Bartlett JG, Gilbert DN. The future of antibiotics and resistance. *N Engl J Med* 2013;**368**:299−302.
191. Berendonk TU, Manaia CM, Merlin C, Fatta-Kassinos D, Cytryn E, Walsh F, et al. Tackling antibiotic resistance: the environmental framework. *Nat Rev Microbiol* 2015;**13**:310−7.

192. Yuan X, Setyawati MI, Leong DT, Xie J. Ultrasmall Ag^{+}-rich nanoclusters as highly efficient nanoreservoirs for bacterial killing. *Nano Res* 2014;**7**:301−7.
193. Javani S, Lorca R, Latorre A, Flors C, Cortajarena AL, Somoza Á. Antibacterial activity of DNA-stabilized silver nanoclusters tuned by oligonucleotide sequence. *ACS Appl Mater Interfaces* 2016;**8**:10147−54.
194. Zheng K, Setyawati MI, Leong DT, Xie J. Antimicrobial gold nanoclusters. *ACS Nano* 2017;**11**:6904−10.
195. Zheng K, Xie J. Composition-dependent antimicrobial ability of full-spectrum Au_xAg_{25-x} alloy nanoclusters. *ACS Nano* 2020;**14**:11533−41.
196. Wang S, Wang Y, Peng Y, Yang X. Exploring the antibacteria performance of multicolor Ag, Au, and Cu nanoclusters. *ACS Appl Mater Interfaces* 2019;**11**:8461−9.
197. Chen WY, Lin JY, Chen WJ, Luo L, Wei G, Diau EWG, et al. Functional gold nanoclusters as antimicrobial agents for antibiotic-resistant bacteria. *Nanomedicine* 2010;**5**:755−64.
198. Miao H, Zhong D, Zhou Z, Yang X. Papain-templated Cu nanoclusters: assaying and exhibiting dramatic antibacterial activity cooperating with H_2O_2. *Nanoscale* 2015;**7**:19066−72.
199. Zheng K, Setyawati MI, Lim TP, Leong DT, Xie J. Antimicrobial cluster bombs: silver nanoclusters packed with daptomycin. *ACS Nano* 2016;**10**:7934−42.
200. Benkovic SJ, Hammes SS. A perspective on enzyme catalysis. *Science* 2003;**301**:1196−202.
201. Strooper BD, Vassar R, Golde T. The secretases: enzymes with therapeutic potential in Alzheimer disease. *Nat Rev Neurol* 2010;**6**:99−107.
202. Lin Y, Ren J, Qu X. Nano-gold as artificial enzymes: hidden talents. *Adv Mater* 2014;**26**:4200−17.
203. Wei H, Wang E. Nanomaterials with enzyme-like characteristics (nanozymes): next-generation artificial enzymes. *Chem Soc Rev* 2013;**42**:6060−93.
204. Meng X, Zare I, Yan X, Fan K. Protein-protected metal nanoclusters: an emerging ultra-small nanozyme. *Wires Nanomed Nanobi* 2020;**12**:e1602.
205. Wang XX, Wu Q, Shan Z, Huang QM. BSA-stabilized Au clusters as peroxidase mimetics for use in xanthine detection. *Biosens Bioelectron* 2011;**26**:3614−9.
206. Hu L, Yuan Y, Zhang L, Zhao J, Majeed S, Xu G. Copper nanoclusters as peroxidase mimetics and their applications to H_2O_2 and glucose detection. *Anal Chim Acta* 2013;**762**:83−6.
207. Li W, Chen B, Zhang H, Sun Y, Wang J, Zhang J, et al. BSA-stabilized Pt nanozyme for peroxidase mimetics and its application on colorimetric detection of mercury (II) ions. *Biosens Bioelectron* 2015;**66**:251−8.
208. Jin L, Meng Z, Zhang Y, Cai S, Zhang Z, Li C, et al. Ultrasmall Pt nanoclusters as robust Peroxidase mimics for colorimetric detection of glucose in human serum. *ACS Appl Mater Interfaces* 2017;**9**:10027−33.
209. Hu D, Sheng Z, Fang S, Wang Y, Gao D, Zhang P, et al. Folate receptor-targeting gold nanoclusters as fluorescence enzyme mimetic nanoprobes for tumor molecular colocalization diagnosis. *Theranostics* 2014;**4**:142.
210. Zhao Q, Huang H, Zhang L, Wang L, Zeng Y, Xia X, et al. Strategy to fabricate naked-eye readout ultrasensitive plasmonic nanosensor based on enzyme mimetic gold nanoclusters. *Anal Chem* 2015;**88**:1412−8.
211. Tiwari JN, Nath K, Kumar S, Tiwari RN, Kemp KC, Le NH, et al. Stable platinum nanoclusters on genomic DNA−graphene oxide with a high oxygen reduction reaction activity. *Nat Commun* 2013;**4**:2221.
212. Fan J, Yin JJ, Ning B, Wu X, Hu Y, Ferrari M, et al. Direct evidence for catalase and peroxidase activities of ferritin−platinum nanoparticles. *Biomaterials* 2011;**32**:1611−8.
213. Hamasaki T, Kashiwagi T, Imada T, Nakamichi N, Aramaki S, Toh K, et al. Kinetic analysis of superoxide anion radical-scavenging and hydroxyl radical-scavenging activities of platinum nanoparticles. *Langmuir* 2008;**24**:7354−64.
214. Tao Y, Lin Y, Huang Z, Ren J, Qu X. Incorporating graphene oxide and gold nanoclusters: a synergistic catalyst with surprisingly high peroxidase-like activity over a broad pH range and its application for cancer cell detection. *Adv Mater* 2013;**25**:2594−9.
215. Fu Y, Zhao X, Zhang J, Li W. DNA-based platinum nanozymes for peroxidase mimetics. *J Phys Chem C* 2014;**118**:18116−25.
216. Zheng C, Zheng AX, Liu B, Zhang XL, He Y, Li J, et al. One-pot synthesized DNA-templated Ag/Pt bimetallic nanoclusters as peroxidase mimics for colorimetric detection of thrombin. *Chem Commun* 2014;**50**:13103−6.
217. Fisher DE. Apoptosis in cancer therapy: crossing the threshold. *Cell* 1994;**78**:539−42.
218. Czabotar PE, Lessene G, Strasser A, Adams JM. Control of apoptosis by the BCL-2 protein family: implications for physiology and therapy. *Nat Rev Mol Cell Biol* 2014;**15**:49−63.
219. Zhao F, Zhao Y, Liu Y, Chang X, Chen C, Zhao Y. Cellular uptake, intracellular trafficking, and cytotoxicity of nanomaterials. *Small* 2011;**7**:1322−37.
220. Liu Y, Liang J, Wang Q, He Y, Chen Y. Copper nanoclusters trigger muscle cell apoptosis and atrophy *in vitro* and *in vivo*. *J Appl Toxicol* 2016;**36**:454−63.
221. Blackmond DG. The origin of biological homochirality. *CSH Perspect Biol* 2010;**2**:002147.
222. Farrag M, Tschurl M, Heiz U. Chiral gold and silver nanoclusters: preparation, size selection, and chiroptical properties. *Chem Mater* 2013;**25**:862−70.
223. Zhang C, Wang K, Li C, Liu Y, Fu H, Pan F, et al. Stress-induced cytotoxicity of chiral Ag nanoclusters. *J Mater Chem B* 2014;**2**:6931−8.
224. Zhang C, Zhou Z, Zhi X, Ma Y, Wang K, Wang Y, et al. Insights into the distinguishing stress-induced cytotoxicity of chiral gold nanoclusters and the relationship with GSTP1. *Theranostics* 2015;**5**:134.
225. Zhang XD, Wu D, Shen X, Liu PX, Fan FY, Fan SJ. *In vivo* renal clearance, biodistribution, toxicity of gold nanoclusters. *Biomaterials* 2012;**33**:4628−38.
226. Wang J, Chen J, Yang J, Wang H, Shen X, Sun YM, et al. Effects of surface charges of gold nanoclusters on long-term *in vivo* biodistribution, toxicity, and cancer radiation therapy. *Int J Nanomed* 2016;**11**:3475−85.
227. Wang H, Zhao Z, Liu Y, Shao C, Bian F, Zhao Y. Biomimetic enzyme cascade reaction system in microfluidic electrospray microcapsules. *Sci Adv* 2018;**4**:2816.
228. Yu Y, Shang L, Guo J, Wang J, Zhao Y. Design of capillary microfluidics for spinning cell-laden microfibers. *Nat Protoc* 2018;**13**:2557−79.
229. Loynachan CN, Soleimany AP, Dudani JS, Lin Y, Najer A, Bekdemir A, et al. Renal clearable catalytic gold nanoclusters for *in vivo* disease monitoring. *Nat Nanotechnol* 2019;**14**:883−90.